One for all – Human kidney Caki-1 cells are highly susceptible to infection with corona- and other respiratory viruses

Daniels A.[1,2,◊], Fletcher S. [1,◊], Kerr H.[1], Kratzel A.[3,4], Pinto, R.M. [1], Kriplani N.[1,♠], Craig N.[1], Hastie C.J.[5], Davies P.[5], Digard P.[1], Thiel V.[3,4], Tait-Burkard C.[1]*

[1]The Roslin Institute, Royal (Dick) School of Veterinary Studies, University of Edinburgh, Easter Bush, Midlothian, United Kingdom.

[2]Infection Medicine, University of Edinburgh, Little France Crescent, United Kingdom.

[3]Institute of Virology and Immunology (IVI), Bern, Switzerland.

[4]Department of Infectious Diseases and Pathobiology, Vetsuisse Faculty, University of Bern, Bern, Switzerland.

[5]Medical Research Council Protein Phosphorylation and Ubiquitylation Unit, College of Life Sciences, University of Dundee, Dundee, United Kingdom.

*Corresponding author

Email: christine.burkard@roslin.ed.ac.uk

◊ These authors contributed equally to this work.

♠Currently: Milteny Biotec, United Kingdom

Abstract

In vitro investigations of host-pathogen interactions of viruses are reliant on suitable cell and tissue culture models. Results are only as good as the model they have been generated in. However, choosing cell models for *in vitro* work often depends on what is available in labs or what has previously been used. Despite the vast increase in coronavirus research activity over the past few years, researchers are still heavily reliant on: non-human cells, for example Vero E6, highly heterogeneous or not fully differentiated cells, such as Calu-3, or naturally unsusceptible cells requiring overexpression of receptors and other accessory factors, such as ACE2 and TMPRSS2. Complex cell models, such as primary cell-derived air-liquid interface epithelial models are highly representative of human tissues but are expensive and time-consuming to develop and maintain. They have limited suitability for large-scale and high-throughput analysis.

Using tissue-specific expression pattern as a selection criteria, we identified human kidney cells as an ideal target for severe acute respiratory syndrome coronavirus-2 (SARS-CoV-2) and broader coronavirus infection. We show the use of the highly characterized human kidney cell line Caki-1 for infection with three human coronaviruses: *Betacoronaviruses* SARS-CoV-2 and Middle Eastern respiratory syndrome coronavirus (MERS-CoV) and *Alphacoronavirus* human coronavirus 229E (hCoV-229E). Caki-1 cells show equal or superior susceptibility to all three coronaviruses when compared to other commonly used cell lines for the cultivation of the respective virus. Antibody staining against SARS-CoV-2 N protein shows comparable replication rates. Using a panel of 21 antibodies in infected Caki-1 cells using immunocytochemistry shows the location of viral proteins during replication. In addition, Caki-1 cells were found to be susceptible to two other human respiratory viruses, influenza A virus and respiratory syncytial virus, making them an ideal model for cross-comparison of not only a broad range of coronaviruses but respiratory viruses in general.

Author Summary

Investigating how viruses interact with their host relies models used for laboratory research. The closer a model matches the host, the more conclusive results are. Complex cell systems based on primary epithelial or stem cells are the gold standard of *in vitro* research. However, they are expensive, time consuming, and laborious to establish. Therefore, cell lines remain the backbone of virus research.

Despite vastly increased research into human coronaviruses following the COVID-19 pandemic, researchers continue to rely on suboptimal cell line models, for example ells of non-human origin like the VeroE6 African Green Monkey cell line. Using known expression patterns of the entry factors of the COVID-19 causative agent severe acute respiratory syndrome coronavirus-2 (SARS-CoV-2) we identified the Caki-1 cell line as a target for SARS-CoV-2. This cell line could be shown to be infectable with a wide range of coronaviruses including common cold virus hCoV-229E, epidemic virus MERS-CoV, and SARS-CoV-2 as well as other important respiratory viruses influenza A virus and respiratory syncytial virus. We could show that SARS-CoV-2 proteins can be stained for and localized in Caki-1 cells and the cells are competent of forming a cellular immune response. Together, this makes Caki-1 cells a unique tool for cross-virus comparison in one cell line.

Introduction

Coronaviruses are a family of enveloped, positive-sense RNA viruses within the order *Nidovirales.* They are split into four genera: alpha-, beta-, delta-, and gamma- coronaviruses. *Alpha-* and *Betacoronaviruses* mainly infect mammalian hosts while the *Delta-* and *Gammacoronaviruses* primarily infect avian hosts [1]. Four members of the human coronaviruses (hCoV) cause mild, cold-like, upper respiratory infections: *Alphacoronaviruses* -229E and -NL63 and *Betacoronaviruses* -HKU1 and -OC43. On three occasions in the last 20 years, zoonotic transmission events of *Betacoronaviruses* lead to epidemic and pandemic disease outbreaks with higher severity pathologies: Severe acute respiratory syndrome coronavirus (SARS-CoV) in 2002-2003 [2]; Middle Eastern respiratory syndrome coronavirus (MERS-CoV) 2012-ongoing [3]; and most recently SARS-CoV-2, the causative agent of the coronavirus disease 2019 (COVID-19) pandemic 2019-ongoing [4]. The potential for future zoonotic events increases as human-animal reservoir interaction increases, for example through population growth, displacement due to climate change, deforestation, and finding alternative food sources.

Understanding coronavirus infections and host-pathogen interaction is paramount to developing novel antiviral strategies, and to prepare for future epidemics. This makes it imperative to find robust cell line models that are widely permissive to different coronaviruses allowing for direct comparison increasing result validity.

Important criteria for selecting model cell lines include species origin, tissue relevance, method of immortalization (i.e. presence of overexpressed viral oncogenes), genetic characterization and karyotype, versatility, and ease of culturing. A number of cell lines were identified as being naturally permissive to SARS-CoV-2, most notably Vero E6, Caco-2, and Calu-3 cells [5]. Overexpression of the main viral entry receptor, angiotensin-converting enzyme 2 (ACE2), sometimes aided by the overexpression of the proteolytic processing factor transmembrane protease, serine 2 (TMPRSS2) was shown to render non-susceptible cell lines permissive to SARS-CoV-2 infection. Although the overexpression cell lines then are permissive to infection, there are limitations and drawbacks to their use in research. Most notably, Vero E6 cells, which have been shown to be susceptible to many human viruses including influenza A virus (IAV), SARS-CoV, and MERS-CoV, are of African Green Monkey (*Chlorocebus aethiops*) origin, making them a less clinically relevant model. More importantly, they are deficient in type I interferon production due to a large deletion in their genome [6]. Tissue culture adaptation mutations and attenuation in the viral genome, such as the loss of the S1/S2 furin-cleavage site in SARS-CoV-2 spike (S), have been observed when the virus was passaged on Vero E6 cells [7]. Although the other notable cell lines commonly used to study SARS-CoV-2 are of human origin, viral titers obtained from Calu-3 and Caco-2 are lower than in Vero E6 cells [8]. Calu-3 and Caco-2 cells are heterogeneous

101 populations of not fully differentiated cells, leading to varied consistency based on culturing
102 methods. Some people also report difficulties culturing Calu-3 cells. Other, less explored cell lines
103 were shown to be susceptible to high-titer SARS-CoV-2 infection, such as the breast cancer cell
104 line CAL-51 [5],

105 The need for consistent and comparable cell lines has been highlighted by results from several
106 genome-scale CRISPR knock-out studies investigating host factors during SARS-CoV-2 infection.
107 The screens used different cell lines including Vero E6 [9], A549-ACE2 [10, 11], Huh7.5 [12], or a
108 clone of Huh7.5 modified to overexpress both ACE2 and TMPRSS2 (Huh7.5.1-ACE2-IRES-
109 TMPRSS2) [13]. Of these studies, ACE2 and cathepsin L (CTSL) were the only gene hits to overlap
110 across all screens. The strongest overlap was observed between screens utilizing the same cell
111 lines [10, 11] or clonal variants of a cell line [12, 13]. Although this suggests that there is
112 reproducibility when using the same cell line, some cell lines modified for overexpression of
113 cellular receptors have limited use for cross-comparison studies between viruses. For instance,
114 while A549-ACE2 cells would be sufficient for comparing SARS-CoV and -2, both of which utilize
115 ACE2, they could not be used to compare to other coronaviruses, such as hCoV-229E utilizing
116 alanyl aminopeptidase (ANPEP) or MERS-CoV utilizing dipeptidyl peptidase 4 (DPP4) during
117 entry. Additional overexpression or selection of clonal populations could change properties when
118 comparing to other viruses. Huh7.5 cells and their derivatives are more broadly useable as they
119 are naturally infectable by both hCoV-229E, and MERS-CoV due to their expressing a wide range
120 of cell surface receptors. However, they are not very robust and exhibit extreme cytopathic effect
121 upon early infection, limiting the types of studies to be conducted in these cells.

122 We aimed to find an adherent cell line that was both easy to transfect and naturally permissible
123 to SARS-CoV-2. Both the human protein ATLAS and gene expression data deposited on NCBI
124 identify the kidney as a tissue with high ACE2 expression. Pathology has furthermore identified
125 SARS-CoV-2 infection within the kidneys of infected patients. Therefore, a human cell line isolated
126 from a male clear cell carcinoma patient, Caki-1 (ATCC HTB-46), which has been previously used
127 in cancer and toxicology studies was identified as a candidate target cell line. It has been well
128 characterized through a number of loss-of-function screens and omics characterizations, as well
129 as having data on drug sensitivities through the use of compound viability screens. A complete
130 list of datasets can be found through the depmap portal
131 (https://depmap.org/portal/cell_line/ACH-000433). Although Caki-1 cells have previously been
132 reported to be permissive to two members of the family *Poxviridae*, myxoma virus [14] and
133 Tanapoxvirus [15], we were unable to find reports of their being tested for infection with any
134 RNA viruses.

135 Here, we describe the successful infection of Caki-1 cells when challenged with coronaviruses
136 SARS-CoV-2, MERS-CoV, and hCoV-229E. All viruses replicated to similar or improved levels
137 compared to commonly used cell lines. Using a SARS-CoV-2 anti-N antibody, we could show
138 comparable replication kinetics between Caki-1 and Vero E6 cells. A panel of 26 antibodies raised
139 in sheep against the known structural and non-structural proteins encoded by SARS-CoV-2 were
140 used to study their cellular location during the SARS-CoV-2 replication in Caki-1 cells. We found
141 good expression of virus receptors, interferon competence and susceptibility to gene knockdown
142 in Caki-1 cells. Furthermore, two other clinically important respiratory RNA viruses, influenza A
143 virus (IAV, order *Articulavirales*), and respiratory syncytial virus (RSV, order *Mononegavirales*)
144 were also found to infect Caki-1 cells to comparable levels with the commonly used cell lines used
145 for these viruses.

146 **Results**

147 To compare the differences between infection in Caki-1 cells and the typical amplification cell line
148 for each coronavirus, time courses of infection were performed for SARS-CoV-2, including
149 variants of concern (VOCs), MERS-CoV, and hCoV-229E.

150 **Caki-1 cells show matching or improved infectability with SARS-CoV-2 compared to Vero**
151 **E6 cells**

152 Cells were infected with SARS-CoV-2 D614G or VOCs alpha, delta, or omicron (BA.1) to investigate
153 how the growth profile differed between clinical isolates from early stages of the pandemic
154 through to the current predominant variant, omicron (Results

155 A). Cells at confluence were inoculated with MOIs 0.1, 1, or 10 as determined by endpoint titration
156 on Vero E6 cells, except for omicron, which was titrated on Caki-1 cells due to poor growth on
157 Vero E6 cells. Following media replacement at 1.5 hours post inoculation (hpi), supernatant
158 samples were collected and viral RNA quantities in the supernatant determined by direct lysis
159 against a standard curve of known titer samples. The European "Original" strain EDB-2 showed a
160 similar replication pattern in Caki-1 and Vero E6 cells at all MOIs. Both reached a plateau at 24 hpi
161 at a relative $TCID_{50}$/ml of ~10^7 and maintained that value until the 120 hpi time point. There was
162 little difference in the log phase for EDB-2 between cell lines and MOIs, although the Vero E6 cells
163 show greater variation across the time points compared to Caki-1 cells in which variation
164 decreases as the MOI increases (Results

165 A). For the alpha variant, first detected in November 2020, we used strain EDB-α-1 for infection.
166 The replication curve in Vero E6 cells flattens into a more linear phenotype peaking at 96 hpi with
167 a relative $TCID_{50}$/ml in the low 10^6 region for all MOIs. The MOI of 0.1 infection lags slightly
168 behind. Contrastingly, viral replication in Caki-1 cells still shows exponential growth, with
169 stratification between the MOIs through the log phase before all plateauing at 48 hpi with a
170 relative $TCID_{50}$/ml maintained at ~10^7 (Results

171 A). For the delta variant, which emerged in late 2020, we used strain EDB-δ-1. The delta variant
172 did not replicate as well as either previous variant overall and shows a more linear growth
173 phenotype, similar to the EDB-α-1 variant in Vero E6, in both Vero E6 and Caki-1 cells. In both
174 cell lines replication plateaus at 72 hpi up to 2-3x10^6 $TCID_{50}$/ml by 96 hpi. For EDB-δ-1, the
175 increase in viral titer across the entire time course, in both cell lines, was only two logs. In
176 contrast, in Caki-1 cells for EDB-2 and EDB-α1 the fold-change was five log_{10} (Results

177 A). The last VOC, omicron, was detected in December 2021 with new subvariants emerging since.
178 Here, using EDB-o-BA.1-10, we saw very poor infection in Vero E6 cells, barely increasing by 10-
179 fold across 120 hpi, and dropping thereafter, likely due to virus degradation. In Caki-1 cells, we

180 see a growth phenotype comparable to the original EDB-2 strain with a log phase peaking at 24
181 hpi and stratification between the different MOIs. Once EDB-o-BA.1-10 reaches a plateau in Caki-
182 1 cells at a $TCID_{50}$/ml of ~10^6, it remains steady with very little variation for the remainder of the
183 time course. Viral replication of EDB-o-BA.1-10 in Caki-1 is reaching higher levels compared to
184 Vero E6 cells (Results

185 A). As the virus evolved, it remained capable of replicating in the Caki-1 cells whilst progressively
186 weaker infection is established in Vero E6 cells. The one exception is EDB-δ-1, which does not
187 replicate well in either cell line.

188 **Caki-1 cells show improved infectability with MERS-CoV and hCoV-229E compared to**
189 **Huh-7**

190 Since Caki-1 cells showed good permissibility to infection with SARS-CoV-2, other coronaviruses
191 were tested to determine if Caki-1 cells could be used as a pan-coronavirus model. To this end,
192 the highly pathogenic beta coronavirus, MERS-CoV, and the less pathogenic common cold alpha
193 coronavirus, hCoV-229E, were tested for replication in Caki-1 cells (Results

194 B+C). The traditional cell line for both these viruses is Huh-7.

195 For MERS-CoV infection, both Caki-1 and Huh-7 cells were inoculated using titres determined on
196 Huh-7 cells. After 2 h, inoculum was replaced and samples taken at indicated time points.
197 Infectious virus produced was assessed by endpoint titration on Huh-7 cells. In initially infected
198 Huh-7 cells, the viral titer for MERS-CoV rose rapidly to 24 hpi and peaks here for an MOI of 1, but
199 is slightly delayed for the lower MOIs, peaking at 48 hpi for 0.1 and 0.01 (Figure 1B). At all MOIs,
200 a peak of ~$1.2x10^7$ $TCID_{50}$/ml titer is achieved. After peaking, a rapid decline is observed for every
201 MOI, crashing down to 10^4 $TCID_{50}$/ml by 96 hpi. Whilst the exponential phase in Caki-1 cells
202 shows initial similarities to Huh-7 the viral titers plateau at 48 hpi for all MOIs. By that time, the
203 cells have managed to support the virus to reach a $TCID_{50}$/ml of ~$2.1x10^9$, which is two logs
204 higher than Huh-7 cells in any condition. Whilst MOIs of 0.1 and 1 show a decreasing titer to ~10^5
205 $TCID_{50}$/ml, MOI 0.01 infectious titers remain high up to 96 hpi. Caki-1 cells show a strong
206 potential with MERS-CoV to be used as a new model system for growing the virus, higher titers
207 are achieved with lower infection concentrations and the titers do not decrease with cell
208 apoptosis as Caki-1 cells can robustly support the infection to its completion.

209 To test whether Caki-1 cells are permissive to hCoV-229E, a GFP-reporter virus was used to
210 measure infection throughout the course of infection using relative fluorescence of GFP as a proxy
211 for viral replication rather than $TCID_{50}$/ml (Results

212 C). Caki-1 and Huh-7 cells were inoculated at indicated virus concentrations as determined on
213 Huh-7 cells. After 1.5 h, inoculum was replaced and plates returned to an incubating plate reader
214 for analysis. The level of fluorescence achieved by both cell lines when infected is comparable to
215 each other, but in Caki-1 cells, we see a quicker and more exaggerated log phase, reaching plateau
216 at roughly 40 hpi, about 10 h before Huh-7 cells. There is also a difference in the lower MOI (0.1),
217 which only achieves a plateau fluorescence value around 5,000 RFU in the Huh-7 cells, a >2-fold
218 reduction compared to Huh-7 cells infected at an MOI of 1, while Caki-1 cells plateau around 8,500
219 RFU, only 2,000 RFU lower than the MOI of 1 and within the margin of error. The Caki-1 cells also
220 show an observable difference of GFP distribution and brightness when compared to Huh-7 cells.
221 Caki-1 cells produce a more uniform phenotype, with less background fluorescence, the GFP is
222 expressed to a greater extent in infected cells, and it takes longer for the cells to round up and lift
223 off the plate. Huh-7 cells generally express the GFP very weakly and in a more punctate fashion,
224 lifting off the plate very early on in infection, making fluorescence readings difficult and
225 inaccurate (data not shown).

226 **Only around 50% of Caki-1 cells get infected by SARS-CoV-2 showing potential of selection**
227 **for even more susceptible subpopulations**

228 To gain greater insight into the infection in Vero E6 cells compared to the more heterogeneous
229 Caki-1 cells, we inoculated the cells at different MOIs (determined on Vero E6 cells) and assessed
230 infection following a single-round infection at 17 hpi through staining for intracellular N protein
231 and analysis by flow cytometry (Figure 1D). For all MOIs analyzed, the level of infected Caki-1
232 cells is roughly half of the infected Vero E6 cells. The Vero E6 population manages to reach up to
233 ~85.3% infected cells by 17 hpi at an MOI=10 and within the margin of error compared to MOI=1,
234 whereas the Caki-1 reach an infection ~46.8%. Another cell line used for SARS-CoV-2 research is
235 Calu-3, an epithelial lung adenocarcinoma cell line with heterogeneous ACE2 expression. The
236 percentage of infected cells remains low in the wild-type Calu-3 population, reaching 6% infection
237 when inoculated at MOI=10 by 24 hpi, and only increasing by 0.8% after 48 hpi. Calu-3's which
238 have been enriched for high expression of ACE2 through staining, fluorescence activated cell
239 sorting, and expansion, showed a marked increase in percentage of infection cells, reaching 21%
240 at an MOI=0.1 at 24 hpi and roughly 50% at all MOIs at 48 hpi (Figure 1D). Whilst Calu-3 cells
241 take longer to establish an infection, if enriched with ACE2 they are capable of reaching infection
242 levels similar to Caki-1 cells although this is most likely through a multi-round infection unlike
243 the single-round infection in Caki-1 cells at 17 hpi.

244 Caki-1 cells are permissible to all tested coronaviruses and in EDB-o-BA.1-1, MERS-CoV and
245 hCoV-229E, show a stronger infection than in Vero E6 and Huh7 cells, respectively. As SARS-CoV-
246 2 VOCs emerged, Caki-1 cells have become a better infection model than the Vero E6 cells. They

247 also provide a good replication model for other coronaviruses and can outperform the standard
248 Huh-7 cells.

249 **Western blot analysis shows comparable rates of replication staining for the SARS-CoV-2**
250 **N protein**

251 To gain a greater understanding of SARS-CoV-2 infection, antibodies were raised in sheep against
252 all major proteins encoded by the SARS-CoV-2 genome (Figure 2A) by the University of Dundee
253 MRC-Protein Phosphorylation Unit [16]. To assess the rate of replication at the protein level, viral
254 replication was observed through western blot analysis against N protein of lysed cells. Briefly,
255 Vero E6 and Caki-1 cells at confluence were inoculated at MOI=1 (as determined on Vero E6 cells)
256 for 1.5h before media replacement. At indicated time points, cells were lysed and subjected to
257 SDS-PAGE and western blot analysis. Quantification of protein levels normalized to beta-actin
258 show comparable replication between Vero E6 cells and Caki-1 cells for EDB-2. As observed in
259 the virus production levels, the replication of EDB-δ-1 was significantly slower with a first plateau
260 reached at 16h, eventually increasing further to 48hpi but significantly lower in comparison to
261 EDB-2 (Figure 2B). A background band could be observed even in uninfected cells at around
262 40kDa overlapping with the signal for beta-actin. This band was found to disappear when a rabbit
263 anti-beta-actin antibody was used in later experiments (data not shown) indicating cross-
264 reaction of the secondary anti-sheep or anti-mouse antibodies.

265 **Localization of viral proteins in Caki-1 cells during replication may pinpoint towards**
266 **functionality**

267 To fully characterize the SARS-CoV-2 replication in Caki-1 cells the full panel of 26 antibodies
268 targeting both structural and non-structural proteins of the virus (as described above) were used
269 to localize the proteins at peak infection. Caki-1 cells infected at a MOI=1 with SARS-CoV-2-EDB-2
270 were fixed at 16 hpi and stained with antibodies targeting most non-structural proteins and the
271 known open reading frames in the "structural" section of the genome. A compromise was found
272 using the antibodies, which had varying stock concentrations, at 1 in 200. Concentrations are
273 therefore not comparable and for specific use of an antibody, we recommend further
274 optimization. Further details may be found in the materials and methods section and table 1.
275 Confocal images were acquired as z-stacks on a Zeiss LSM 880 (Airyscan) without use of the
276 airyscan function. Imaging conditions were set for each uninfected, stained background cell with
277 the matching primary antibody. Images depict a maximum projection of the z-stack.

278 Of the open reading frame (ORF)2-10 encoded "structural" proteins, ORF3a and b, ORF6 ORF8
279 and N (ORF9) show the strongest signals above background. Almost all SARS-CoV-2 ORF
280 antibodies show specific staining above background with the exception of E (ORF4) (Figure 2B).
281 The spike receptor binding domain (S RBD), ORF2, shows vesicle-like punctate throughout the

282 cytoplasm with a slight enrichment in the enlarged perinuclear space in some cells. There is little
283 staining for S at the plasma membrane, which is in agreement with previous findings showing
284 that only roughly 20% of coronavirus S protein may be found at the plasma membrane in the
285 presence of M [17, 18]. In contrast to S, the M protein (ORF4) was found to be more perinuclear
286 in localization and more punctate (Figure 2B). The viroporin ORF3a, shows similar though
287 stronger punctate staining with concentration around the perinuclear space. This agrees with
288 current SARS-CoV literature and reports of it being involved in autophagy, localizing to the
289 lysosomes [19, 20]. Although there is some background staining in uninfected Caki-1 cells for
290 ORF3a, the staining in the infected control is significantly stronger and background signal is non-
291 specifically localized indicating non-specific background binding that may be optimized using
292 different staining conditions. The small ORF3b protein, which acts as a potent interferon
293 antagonist, localizes in the distal cytoplasm with some vesicular patterning. ORF3b also shows
294 staining at the plasma membrane particularly along actin filaments. This agrees with reports for
295 SARS-CoV of it being a multi-localized protein due to its shuttling behavior [21]. Co-localization
296 studies with known interaction partners, such as IRF3, may shed further light into the role of
297 ORF3b [22]. The interferon antagonist ORF6, binding and sequestering STAT1, is a known
298 virulence factor of SARS-CoV-2, previously found to localize in the ER and at lysosomal
299 membranes upon overexpression [23, 24]. A similar localization pattern is observed upon
300 infection in Caki-1 cells with perinuclear concentration and distributed puncta throughout the
301 cell. Additional staining could further substantiate localization to specific organelles (Figure 2B).
302 SARS-CoV-2 ORF7a and ORF7b are type-I transmembrane proteins also involved in antagonism
303 of the interferon response. Both are expressed and retained intracellularly. Background staining
304 is observed for both these antibodies in the uninfected Caki-1 cells, but the fluorescence is
305 stronger in the infected cells. ORF7a shows vesicular, diffuse localization, whilst ORF7b is
306 concentrated in the perinuclear space with some plasma membrane staining. Little is known
307 about the function of the two proteins, but for example ORF7b was shown to be incorporated into
308 SARS-CoV particles [25]. The protein encoded by the SARS-CoV-2 ORF8 gene is unique to SARS-
309 CoV-2 containing a predicted Ig-like fold, which can interact with a variety of host proteins
310 involved in ER-associated degradation. Caki-1 cells show a strong staining with no background in
311 the uninfected cells, and we see a vesicular staining with a concentration towards the plasma
312 membrane in agreement with the existing literature showing secretion of ORF8 [26]. ORF9, the
313 nucleocapsid protein (N), shows localization to the replication-transcription complex in the
314 perinuclear space, where it aids packaging of the viral genome into a ribonucleoprotein particle.
315 Staining for N is abundant across the cell, and even shows a small amount of nuclear staining (the
316 seemingly stronger nuclear staining visible in the image is a consequence of maximum
317 projection). N is also secreted into the extracellular space in larger amounts than ORF8, indicated

318 by some of the vesicular and distal staining [27, 28]. An alternative ORF located within the N gene
319 is ORF9b, which plays a role in suppressing innate immunity. ORF9b shows a very diffuse staining
320 across the cell with no background in the uninfected cells. Reports have linked this protein with
321 the mitochondrial membrane [29, 30], and upon close inspection, long punctate networks can be
322 seen within some of the staining, although this is not obvious indicating mitochondrial interaction
323 not to be a primary function of the protein. Most importantly, ORF9b shows clear nuclear
324 localization. An second alternative ORF located within N encodes for ORF9c, a membrane-
325 associated protein and has been associated with antiviral response suppression and suggested to
326 be unstable [31]. Our results show an interesting concentration of ORF9c protein at the end of
327 what look to be actin protrusions. Accumulations near the nucleus could however indicate an
328 unfolded protein response (Figure 2B). ORF10 is possibly one of the most obscure proteins of
329 SARS-CoV-2, with little known about its function. We found some perinuclear aggregations of the
330 protein and otherwise relatively evenly distributed small puncta throughout the cell (Figure 2B).

331 The SARS-CoV-2 non-structural proteins (NSPs) are generated through proteolytic cleavage of
332 the ORF1a and ORF1ab polyproteins. Of these, NSPs 3, 8, 10 and 16 gave the clearest staining.
333 However, some NSPs showed very little specific staining, primarily NSP9 for which no staining
334 could be seen in infected Caki-1 cells (Figure 3). The N-terminal cleavage products NSP1 and NSP2
335 are conserved across the coronavirus family and are both involved in halting host translation
336 [32]. Whilst NSP1 shows very sparse staining in very distinct puncta throughout the cytosol,
337 staining for NSP2 is concentrated around the perinuclear space. NSP3 is responsible for cleavage
338 of NSP1, NSP2, and NSP3 from the N-terminal region of the polyproteins [33], and shows
339 widespread, punctate staining. Some cells, possibly at an earlier stage in their infection cycle,
340 show a more perinuclear focused staining, likely co-localizing with the replication transcription
341 complex (RTC). The main proteinase NSP5 shows a very strong perinuclear, likely RTC,
342 phenotype. NSP8 and NSP7 form a heterodimer. It is then unsurprising that staining for the
343 proteins show similar localization. Whilst NSP7 is a relatively weak signal, NSP8 exhibits strong
344 perinuclear staining showing big spots of protein staining, defined by its role in the RTC [34].
345 NSP8 also shows some nuclear staining, however, since there is some background nuclear
346 staining it is unlikely this is a real signal (Figure 3). The growth-factor-like protein NSP10, which
347 serves as a stimulatory factor for NSP14-ExoN [35], shows broadly distributed punctate staining
348 with some localization to the plasma membrane and although the staining for NSP14 is not as
349 strong, it demonstrates a similar pattern but with no membrane localization. NSP11_12, the latter
350 being the RNA-dependent-RNA-polymerase, shows staining localizing to the RTC, as do the
351 helicase NSP13, the endoribonuclease NSP15. There may be some staining for NSP13 in the

352 nucleus. NSP16, a methyltransferase, shows nuclear staining and punctate staining throughout
353 the cytosol indicating vesicular localization, and potentially some secretion [36] (Figure 3).

354 **Caki-1 cells show expression of receptors linked to SARS-CoV-2 and other human**
355 **coronaviruses**

356 To further understand the suitability of Caki-1 cells for infection assays and to account for the
357 high permissibility to many coronaviruses, receptor expression profiling, interferon competence
358 and siRNA knockdowns were conducted. The receptors/entry proteins for SARS-CoV-2,
359 MERS-CoV and hCoV-229E, were checked for mRNA quantity by RT-qPCR, and normalized
360 against a housekeeping gene (RRN18S) (Figure 1**: Time course assays in coronaviruses**
361 **comparing the most commonly used cell line with Caki-1.** For all graphs: circle points = MOI
362 10, square points = MOI 1, triangle points = MOI 0.1, diamond points = MOI 0.01, and the darker
363 the color the higher the MOI, error bars indicate +/- SEM. [A] Time course infection of SARS-CoV-
364 2 variants on Vero E6 and Caki-1 cells, biological n=3x3. Measured through RT-qPCR for the SARS-
365 CoV-2 N gene in the supernatant, samples taken at 0, 6, 16, 24, 48, 72, 96 and 120 hpi at MOIs of
366 10, 1 and 0.1. [B] Time course infection of MERS-CoV on Huh-7 and Caki-1 cells, biological n=3x3,
367 measured through TCID50 on Huh-7 cells. Samples taken at 24h intervals until 96hpi. [C] GFP
368 time course of infection for hCoV-229E on Huh-7 and Caki-1 cells, measured from 0 hpi to 78 hpi
369 in 6 h intervals, with fluorescence as a proxy for viral replication, biological n=3x3. [D]
370 Fluorescence-activated cell sorting to determine the percentage of infected SARS-CoV-2 cells in
371 Vero E6, Caki-1, Calu-3 and Calu-3-ACE2 cells. Vero E6 and Caki-1 cells were fixed at 17 hpi,
372 stained for intracellular SARS-CoV-2 N protein and sorted for fluorescent cells, biological n=3x3.
373 The same was conducted for Calu-3 and Calu-3-ACE2 cells at 24 hpi and 48 hpi, biological n=3x3.

374 A). NRP1 (SARS-CoV-2 attachment), ANPEP (hCoV-229E receptor) and DPP4 (MERS-CoV
375 receptor) all showed a similar level of relative expression in Caki-1 cells demonstrating that they
376 are actively being expressed. Levels of around 1,000-fold lower expression than a housekeeping
377 gene are in alignment with expression levels previously determined in lung (e.g. DPP4 [37]). ACE2
378 (SARS-CoV-2 receptor) and TMPRSS2 (one of the SARS-CoV-2 spike modifying proteases) had a
379 relative lower amount of mRNA than the other factors, but this pattern correlates with expression
380 of these proteins in nasal epithelial cells [38], perhaps providing an indication as to why they are
381 so readily infectable with SARS-CoV-2.

382 **Caki-1 cells can be readily transfected with siRNA**

383 To confirm Caki-1 cells are suitable cells in which to perform transfection experiments the effect
384 of siRNA transfection targeting known entry factors of SARS-CoV-2 was examined by reading viral
385 release 96 h post transfection (hpt) and 24 hpi (Figure 4B). A panel of genes implicated in
386 SARS-CoV-2 entry (ACE2, TMPRSS2, NRP1, CTSB, CTSL), and a virus specific gene (SARS-CoV-2

387 N) were knocked down before infection with EDB-2 at 72 hpt. All genes showed a significant
388 (****p<0.0001) reduction in replication compared to non-targeting siRNA, with SARS-CoV-2 N
389 and NRP1 showing the strongest phenotypes with a relative replication compared to the
390 non-targeting control of 8 and 9% respectively. Knockdown of CTSB had the least effect on viral
391 replication, only causing a 50% reduction in released virus, followed by TMPRSS2 at 24.7%
392 relative replication. The viability of the Caki-1 cells after knockdown was measured by
393 fluorescence created through mitochondrial metabolism as a proxy for cell viability. There was
394 no difference to cell viability after knockdown of any of these genes. Neither was there any effect
395 on cell viability due to being treated with the transfection reagent (Mock). This shows that Caki-1
396 cells can be transfected successfully and that it results in the desired effect on viral replication,
397 they can also tolerate the transfection reagent without a reduction in cell viability. Knockdowns
398 were validated by RT-qPCR and showed at least 80% reduction in mRNA (data not shown).

399 **Caki-1 cells are interferon competent**

400 Many cancer cells lines are deficient in their interferon response, especially Vero E6 cells, which
401 lack the ability to produce interferon through a large deletion in their genome [6]. This can be
402 detrimental for studying a fully comprehensive viral replication cycle, as close to natural infection
403 as possible in a cancer cell line. It often also drives viral adaptation over serial passaging of field
404 isolates. To assess the interferon response in Caki-1 cells, and therefore their suitability as a good
405 infection model for SARS-CoV-2, we stimulated them with Poly I:C and LPS and measured their
406 IFNα/β output by HEK-Blue IFNα/β assay (Figure 1**: Time course assays in coronaviruses**
407 **comparing the most commonly used cell line with Caki-1.** For all graphs: circle points = MOI
408 10, square points = MOI 1, triangle points = MOI 0.1, diamond points = MOI 0.01, and the darker
409 the color the higher the MOI, error bars indicate +/- SEM. [A] Time course infection of SARS-CoV-
410 2 variants on Vero E6 and Caki-1 cells, biological n=3x3. Measured through RT-qPCR for the SARS-
411 CoV-2 N gene in the supernatant, samples taken at 0, 6, 16, 24, 48, 72, 96 and 120 hpi at MOIs of
412 10, 1 and 0.1. [B] Time course infection of MERS-CoV on Huh-7 and Caki-1 cells, biological n=3x3,
413 measured through TCID50 on Huh-7 cells. Samples taken at 24h intervals until 96hpi. [C] GFP
414 time course of infection for hCoV-229E on Huh-7 and Caki-1 cells, measured from 0 hpi to 78 hpi
415 in 6 h intervals, with fluorescence as a proxy for viral replication, biological n=3x3. [D]
416 Fluorescence-activated cell sorting to determine the percentage of infected SARS-CoV-2 cells in
417 Vero E6, Caki-1, Calu-3 and Calu-3-ACE2 cells. Vero E6 and Caki-1 cells were fixed at 17 hpi,
418 stained for intracellular SARS-CoV-2 N protein and sorted for fluorescent cells, biological n=3x3.
419 The same was conducted for Calu-3 and Calu-3-ACE2 cells at 24 hpi and 48 hpi, biological n=3x3.

420 C). Stimulation with a transfection reagent only (DF1) induced a small response, comparable to
421 cells cultured in media containing Poly I:C. Caki-1 cells only showed a very small response to LPS

422 stimulation, comparable to other stimulant addition. However, when Poly I:C was transfected to
423 mimic a viral infection, IFN α/β production rose dramatically from 0.0004 μg/ml for DF1 only to
424 0.2 μg/ml for 1 μg/ml Poly I:C (****p<0.0001) and 0.08 μg/ml for 10 μg/ml Poly I:C (***p<0.001).
425 None of the other conditions provided a significant difference from untreated. This demonstrates
426 that Caki-1 cells can mount a competent interferon response, and so, in assays which investigate
427 interferon pathways in viral replication, and any other host-pathogen interactions, they would
428 provide a complete picture of viral replication.

429 **Caki-1 cells are broadly susceptible to infection with other respiratory viruses RSV and IAV**
430 To determine whether Caki-1 cells are permissible to infection with other respiratory viruses not
431 in the coronavirus family, they were infected with either the IAV H1N1 vaccine strain A/Puerto
432 Rico/8/1934 (H1N1 PR8), a more recent H1N1 isolate A/Norway/3433/2018 (H1N1 Norway
433 2018), or RSV and compared to the standard cell line used to replicate these viruses. In a trypsin-
434 dependent infection with both H1N1 strains, Caki-1 cells supported virus replication comparably
435 to MDCK cells when infected with an MOI=0.001. No infection was observed in a trypsin-
436 independent infection (data not shown). Slightly lower levels of infectious virus were found in
437 Caki-1 cells up to 24 and 48 hpi for H1N1 Norway and PR8, respectively (Figure 1**: Time course**
438 **assays in coronaviruses comparing the most commonly used cell line with Caki-1.** For all
439 graphs: circle points = MOI 10, square points = MOI 1, triangle points = MOI 0.1, diamond points
440 = MOI 0.01, and the darker the color the higher the MOI, error bars indicate +/- SEM. [A] Time
441 course infection of SARS-CoV-2 variants on Vero E6 and Caki-1 cells, biological n=3x3. Measured
442 through RT-qPCR for the SARS-CoV-2 N gene in the supernatant, samples taken at 0, 6, 16, 24, 48,
443 72, 96 and 120 hpi at MOIs of 10, 1 and 0.1. [B] Time course infection of MERS-CoV on Huh-7 and
444 Caki-1 cells, biological n=3x3, measured through TCID50 on Huh-7 cells. Samples taken at 24h
445 intervals until 96hpi. [C] GFP time course of infection for hCoV-229E on Huh-7 and Caki-1 cells,
446 measured from 0 hpi to 78 hpi in 6 h intervals, with fluorescence as a proxy for viral replication,
447 biological n=3x3. [D] Fluorescence-activated cell sorting to determine the percentage of infected
448 SARS-CoV-2 cells in Vero E6, Caki-1, Calu-3 and Calu-3-ACE2 cells. Vero E6 and Caki-1 cells were
449 fixed at 17 hpi, stained for intracellular SARS-CoV-2 N protein and sorted for fluorescent cells,
450 biological n=3x3. The same was conducted for Calu-3 and Calu-3-ACE2 cells at 24 hpi and 48 hpi,
451 biological n=3x3.

452 D).

453 HEp-2 cells are typically used to expand RSV. Caki-1 and HEp-2 cells were inoculated with a
454 fluorescence reporter virus RSV-A2-GFP. Replication was measured as a proxy by measuring the
455 florescence reporter in an incubating plate reader. For the first time, the replication in Caki-1 cells
456 does not match or outperform replication of RSV in HEp-2 cells (Figure 1**: Time course assays**

457 **in coronaviruses comparing the most commonly used cell line with Caki-1.** For all graphs:
458 circle points = MOI 10, square points = MOI 1, triangle points = MOI 0.1, diamond points = MOI
459 0.01, and the darker the color the higher the MOI, error bars indicate +/- SEM. [A] Time course
460 infection of SARS-CoV-2 variants on Vero E6 and Caki-1 cells, biological n=3x3. Measured through
461 RT-qPCR for the SARS-CoV-2 N gene in the supernatant, samples taken at 0, 6, 16, 24, 48, 72, 96
462 and 120 hpi at MOIs of 10, 1 and 0.1. [B] Time course infection of MERS-CoV on Huh-7 and Caki-
463 1 cells, biological n=3x3, measured through TCID50 on Huh-7 cells. Samples taken at 24h intervals
464 until 96hpi. [C] GFP time course of infection for hCoV-229E on Huh-7 and Caki-1 cells, measured
465 from 0 hpi to 78 hpi in 6 h intervals, with fluorescence as a proxy for viral replication, biological
466 n=3x3. [D] Fluorescence-activated cell sorting to determine the percentage of infected SARS-CoV-
467 2 cells in Vero E6, Caki-1, Calu-3 and Calu-3-ACE2 cells. Vero E6 and Caki-1 cells were fixed at 17
468 hpi, stained for intracellular SARS-CoV-2 N protein and sorted for fluorescent cells, biological
469 n=3x3. The same was conducted for Calu-3 and Calu-3-ACE2 cells at 24 hpi and 48 hpi, biological
470 n=3x3.

471 E). However, the infection in Caki-1 cells outperforms RSV infection in A549 cells through faster
472 and stronger (higher fluorescence) growth. The fluorescence from the HEp-2 cells (turquoise)
473 reaches 7,000 RFU for MOIs of 1 and 0.1, with 0.1 remaining slightly under MOI=1 for the entire
474 replication cycle (0 hpi – 78 hpi). Although the Caki-1 cells do show a logarithmic replication
475 curve at both MOIs, it is shallow and plateaus by 42 hpi, about 10 h before the HEp-2 cells. The
476 maximum RFU achieved by the hRSV-A2-GFP is ~3,700, about half of the RFU achieved in HEp-2.
477 The variation at the later timepoints has increased compared to HEp-2 cells. No syncytia
478 formation was observed in the Caki-1 cells upon hRSV-A2-GFP infection, but CPE was present at
479 48 hpi.

480 **Discussion**

481 Here we have shown that Caki-1 cells can be used to model infection for a range of respiratory
482 viruses; SARS-CoV-2, CoV-229e, MERS-CoV, IAV, and RSV. With the exception of RSV, they are
483 comparable to or outperform the current preferred cell line for viral production, whilst also
484 providing a naturally permissible environment for the virus to replicate in. They express all the
485 receptors needed for infection with SARS-CoV-2, MERS-CoV, and hCoV-229E, and are responsive
486 to transfection with siRNA without significant cell death. They have a competent interferon
487 response as demonstrated by stimulation with Poly I:C and are also permissive to other
488 respiratory viruses. This makes them a highly useful model for direct comparison of respiratory
489 viruses across one, unmodified (no overexpression) cell line.

490 The natural susceptibility of Caki-1 (human) cells to a range of respiratory viruses, although not
491 a lung cell line, provides them with an advantage over many other cell lines used for viral
492 research. Particularly over the much used Vero E6 cells (African Green Monkey), which, although
493 permissive to many different viruses, do not provide a representative environment for human
494 pathogens. The broad susceptibility of Caki-1 cells to respiratory virus infection allows for their
495 use in comparative studies between viruses. Calu-3 cells, which have been widely used as a lung
496 cell model for SARS-CoV-2, show a very low percentage infection and are difficult to grow.
497 Selection for ACE2 expressing cells (Calu-3-ACE2) through FACS makes the cells more permissive
498 to infection with SARS-CoV-2 and can also enhance growth characteristics through selection of
499 cell subpopulations. However, this specializes the Calu-3-ACE2 cells to infection with SARS-CoV-2
500 and is likely impacting infectability with other viruses. Similarly though, if someone wanted a
501 more highly permissive version of Caki-1cells to study their SARS-CoV-2 infection, selection of
502 ACE2 cells may improve infection beyond 50%. We would however advise to keep this population
503 as is due to its broad susceptibility to a range of respiratory viruses.

504 Whilst Caki-1 are still a cancer cell line, and thus contain the mutations and caveats associated
505 with that fact, they have a well-characterized genome and expression patterns. Whilst they have
506 a knockout mutation in the CDKN2 gene and this should be kept in mind, they also boast a fully
507 receptive innate immune response, allowing this pathway to be interrogated
508 (https://www.cbioportal.org/, Accessed 8/10/2022, [39, 40]). This is also demonstrated by their
509 response to intracellular Poly I:C (a viral mimic), but not to LPS which is a bacterial stimulant of
510 immune cells, showing their response is specific and relevant to viral infections. Conversely, the
511 Vero E6 cells are defective in its production of interferon, but remains sensitive to the action of
512 interferon through ISGs, often making it a preferred cell line for the production of viral stocks,
513 with the caveat that attenuation is more likely [6].

514 With the emergence of new SARS-CoV-2 variants it has been found that in other cell lines, there
515 is a change in tropism and attachment / processing factor preference leading to a loss of infection
516 [41]. Caki-1 cells are able to maintain equal levels of infection across all the VOCs tested (alpha,
517 delta, and omicron), without a change in phenotype, whereas Vero E6 cells lose their ability to
518 effectively support viral replication as the variants evolve. This decrease in permissibility of the
519 Vero E6 cells runs in parallel with the decrease in severe symptoms seen with the evolution of
520 the variants, with omicron causing the mildest disease of all the variants, likely attributed to a
521 change in cell tropism and / or temperature [42]. As the Caki-1 cells can support infection of the
522 omicron variant, and it has been reported that omicron has moved away from TMPRSS2 mediated
523 entry [43], it could be assumed that entry into Caki-1 cells is less or not TMPRSS2 dependent. This
524 is reflected in the knockdown phenotypes (Figure 4B) with 25% relative infection still occurring
525 upon knockdown of TMPRSS2. This makes the Caki-1 cell line very valuable for future SARS-CoV-
526 2 research as they will be useful to study the host-virus interactions of variants evolved from
527 omicron.

528 The Caki-1 cell line also offers ideal growth characteristics for viral study and propagation. Whilst
529 being permissive to transfection Caki-1 cells have a doubling time of 36 hours (preventing
530 overgrowth), the cultures can pack tightly to form dense monolayers capable of supporting
531 widespread viral infection, and are robust enough to be able to maintain multi rounds of infection
532 without significant CPE development. Conversely, Vero E6, Calu-3, and Huh7 cells all develop CPE
533 after 24 hpi with SARS-CoV-2, restricting their use [7, 44]. The slower growth of Caki-1 cells
534 compared to all other preferred cell lines, especially Vero E6 cells, also means that they are
535 suitable for producing stocks of slower growing viruses such as the common cold coronaviruses.
536 Here, we have also utilized Caki-1 cells to isolate clinical samples of SARS-CoV-2, specifically
537 omicron, a methodology which usually has been achieved on Vero E6 cells for all major virus
538 types. This negates the worry for mutation accumulation in the S1/S2 furin cleavage site that has
539 been observed in SARS-CoV-2 within a single passage in Vero E6 cells [7]. The ability of Caki-1
540 cells to support robust infection with multiple respiratory viruses shows that this cell line can be
541 useful to study both coronaviruses and common cold viruses in direct comparison. The growth
542 properties of the cells furthermore improve high-throughput readouts and methods through
543 slower growth and overcrowding, reducing background fluorescence and changes to cell
544 properties in a dense cell layer.

545 The SARS-CoV-2 antibodies developed by MRC PPU Dundee form a useful toolset to quantify and
546 visualize viral proteins throughout the replication cycle as we have demonstrated here. We have
547 shown the localization of most viral proteins within Caki-1 cells, which agrees with the literature
548 for other cell lines localization and relevant SARS-CoV homologues [45, 46], and tagged proteins

549 in A549 cells [47]. Contrast to the studies previously performed, here we can show how natural
550 expression of these proteins is characterized in cells where all other viral proteins and cellular
551 interaction partners are regulated through the viral infection. The staining and the advantage of
552 higher resolution techniques show the vast potential to study viral protein function through
553 localization. Particularly interesting will be the function of nuclear localization of NSP16 and
554 ORF9b in particular. The many functions associated with proteins like N, ORF3B, NSP2, and NSP8
555 are indicated through their broad distribution patterns within the cell. With these antibodies
556 being raised in sheep, they are ideal for pairing with other antibodies for co-localization studies.
557 Here, we have used a variety of antibodies purified from different bleeds of the production sheep
558 as they were available to us. Indications are that later bleeds show less background and more
559 specific staining. It is clear that further optimization for some of the staining protocols is
560 warranted for some of the proteins of interest.

561 The multifaceted uses of Caki-1 cells in viral research are clear; they are easy to work with and
562 manipulate in the lab, they can support a range of viruses across multiple rounds of infection, and
563 in most cases outperform the commonly used cell line for each virus. They naturally highly
564 express a wide range of receptors, and possess an interferon response that can both produce and
565 respond, making them an ideal candidate for studying viral infections *in vitro*.

566 **Methods**

567 **Cells & Viruses**

568 Vero E6 (ATCC CRL-1586), Calu-3 (ATCC HTB-55), Huh-7 (JCRB, JCRB0403), HEp-2 (ATCC CCL-
569 23), and MDCK (ATCC CCL-34) cells were maintained as monolayer cultures in Dulbecco's
570 Modified Eagle's Medium (DMEM, Sigma), supplemented with 10% heat inactivated Fetal Bovine
571 Serum (FBS, Gibco), 1X Ultraglutamine-I (Lonza), and 1X Non-essential Amino Acids (NEAA,
572 Lonza) (complete DMEM). Calu-3 cells were supplemented with 1X Sodium Pyruvate (Sigma).
573 Hek-Blue IFN-α/β (InvivoGen) cells were maintained as monolayer cultures in complete DMEM
574 supplemented with 30 µg/ml of blasticidin (Gibco) and 100 µg/ml of Zeocin (Gibco). Caki-1 cells
575 (ATCC HTB-46) were maintained as monolayer cultures in Roswell Park Memorial Institute
576 medium (RPMI, Sigma), supplemented with 10% heat inactivated FBS (Gibco), 1X
577 Ultraglutamine-I (Lonza), and 1X NEAA (Lonza). Cells were maintained at 37°C in 5% CO_2.

578 Samples from confirmed COVID-19 patients were collected by trained healthcare professionals
579 using combined nose-and-throat swabbing. The samples were stored in virus transport medium
580 and sterile filtered through 0.1 µm filters prior to cultivation and isolation on Vero E6 cells.
581 Variant B.1.1.529 (o) was isolated on Caki-1 cells. Samples were anonymized by coding, compliant
582 with Tissue Governance for the South East Scotland Scottish 279 Academic Health Sciences
583 Collaboration Human Annotated BioResource (reference no. SR1452). Virus sequence was
584 confirmed by Nanopore sequencing according to the ARCTIC network protocol
585 (https://artic.network/ncov-2019), amplicon set V3, and validated against the patient isolate
586 sequence. SARS-CoV-2 variants utilized in this study are EDB-2 (B1.5 at the time, now B.1),
587 EDB-α-1 (B.1.1.7), EDB-δ-1 (B.1.617.2), and EDB-o-BA.1-1 (B.1.1.529, BA.1). Infectivity was
588 quantified by endpoint titration on Vero E6 cells, for all isolates apart from o (omicron), which
589 was titrated on Caki-1 cells. All infections in this study were performed using passage 2 from
590 isolation of each variant.

591 hCoV-229E-GFP [48] was propagated on Huh7 cells at 34°C with 5% CO_2 over 72 hours. Infectivity
592 was quantified by endpoint titration on Huh7 cells.

593 hRSV-A2-eGFP [49] (obtained from Juergen Schwarze, University of Edinburgh) was amplified on
594 HEp-2 cells over 72 hours. Infectivity was quantified by endpoint titration on HEp-2 cells.

595 MERS-CoV strain EMC [50] was propagated in VeroB4 cells. Infectivity was quantified by
596 endpoint titration on Huh7 cells as previously described [51].

597 Influenza strain A/Puerto Rico/8/1934 H1N1 (PR8) was generated by reverse genetics as
598 previously described [52]. A/Norway/3433/2018 H1N1 (Norway H1N1) was kindly supplied by
599 the Worldwide Influenza Centre at the Francis Crick Institute, London, made from clinical samples

600 they received from the WHO National Influenza Centre, Department of Virology,
601 Folkehelseinstituttet, Oslo. A working stock was generated in MDCK cells.

602 **Viral Growth Curves**

603 ***SARS-CoV-2***

604 Vero E6 and Caki-1 cells were seeded to confluence in a 24-well plate one day prior to inoculation
605 at differing MOIs for 1 h. At the indicated time point post infection, supernatant was lysed and
606 quantified as previously described [53]. Briefly, the lysate was added to the reaction at 10% total
607 reaction volume and analyzed by RT-qPCR, using SYBR Green GoTaq 1-Step RT-qPCR (Promega)
608 with the SARS-CoV-2 CDC N3 primers (F – GGGAGCCTTGAATACACCAAAA, R –
609 TGTAGCACGATTGCAGCATTG) at 350 nM each to determine viral copy number according to the
610 manufacturer's instructions (annealing at 60°C) on a Stratagene MX3000p qPCR system. To
611 assess viral copy numbers, resulting Cts were analyzed against a standard curve of lysate with
612 known $TCID_{50}$/ml value as well as an RNA template.

613 ***hRSV and hCOV-229E***

614 HEp-2 (RSV), Huh7 (229E), and Caki-1 (both) cells were seeded to confluence in a black, clear
615 bottom 96-well plate one day prior to infection. After inoculation at differing MOIs for 1.5 h,
616 inoculum was removed and replication measured as a function of GFP fluorescence from 6 hpi to
617 72 hpi in 2-hour intervals (BMG Clariostar; excitation: 470-15, dichroic: 492.5, emission: 515-15,
618 bottom optic). Slopes of the linear phase of replication were calculated then normalized to
619 uninfected cells (slope = 1) and the average slope calculated.

620 ***MERS-CoV***

621 Huh7 and Caki-1 cells were seeded to confluence one day prior to infection. After inoculation at
622 differing MOIs for 2 h inoculum was removed and cells were washed three times with PBS. At
623 indicated time points post infection, supernatant was lysed and quantified as previously
624 described. Virus titers were determined by endpoint titration on Huh7 cells inoculated with serial
625 dilution and $TCID_{50}$/ml was visualized using Crystal Violet 72 hpi and calculated by the
626 Spearman–Kärber algorithm.

627 ***IAV***

628 MDCK and Caki-1 cells were seeded to confluence on the day of infection. Once counted, cells were
629 washed with PBS and infected at MOI 0.001. After a 1h adsorption, inoculum was replaced with
630 serum-free medium supplemented with 1 µg/ml tosyl phenylalanyl chloromethyl ketone (TPCK)-
631 treated trypsin (Sigma) and 0.14% BSA fraction V (w/v) (Sigma). Cells were incubated at 37°C
632 and supernatant samples were harvested at the indicated time points.

633 Virus titers were determined by plaque assays in MDCK cells. Briefly, confluent monolayers of
634 MDCK cells were washed with PBS, infected with ten-fold serial dilutions of virus samples
635 performed in serum-free media and incubated at 37°C for 1h. Inoculum was replaced with DMEM
636 including 0.14% BSA (Sigma), 1 µg/ml TPCK-treated trypsin (Thermo) and 1.2% Avicel (Merck).
637 Following a 3-day incubation, overlay was removed and cells were fixed with 4% formaldehyde
638 in PBS and subsequently stained with 0.1% Toluidine Blue (Sigma-Aldrich). Stained plates were
639 washed under tap water and left to dry. Plaques were counted and viral titers were expressed as
640 PFU/ml.

641 **Fluorescent Activated Cell Sorting (FACS) of Calu-3 cells**

642 Calu-3 cells were enriched for high ACE2 expression (Calu-3-ACE2) by FACS using a BD
643 Biosciences FACSAria III Cell Sorter. Cells were detached from a T75 using Gentle Cell Dissociation
644 Reagent (Stemcell Technologies) and recovered in DMEM prior to staining. Recombinant
645 Anti-ACE2 antibody (Abcam, ab272500) was used at 1:500 before staining with Goat anti-Rabbit
646 IgG (H+L) AF647 (Invitrogen, A-21244) at 1:2000. The top 0.1% of cells expressing ACE2 were
647 collected and cultured in conditioned media to recover and expand.

648 **Flow Cytometry**

649 Vero E6, Caki-1, Calu-3, and Calu-3-ACE2 cells were seeded one day prior to inoculation with
650 SARS-CoV-2-EDB-2 at differing MOIs of 10, 1 and 0.1 for 1 h. At the indicated timepoints, the cells
651 were detached from the well using TrypLE Express Enzyme (Gibco) prior to fixation with 4%
652 formaldehyde. The cells were permeabilized using 0.1% Triton-X-100. Using standard
653 immunocytochemistry techniques, primary antibody targeting SARS-CoV-2 N protein (DA114 4th
654 bleed, MRC PPU Dundee, generated as described in [16]) was used at 1:200 (Table 1) before
655 staining with Donkey anti-Sheep AF488 Secondary Antibody (Invitrogen, A-11015) at 1:2000.
656 The cells were analyzed using a B530/30-A filter on a BD Biosciences LSRFortessa X-20 Cell
657 Analyzer.

658 *Table 1: Antibodies targeting SARS-CoV-2 generated by the MRC PPU and respective concentrations used.*

TARGET	ID	BLEED	STOCK CONC. (MG/ML)	IF	FLOW
				Dil. / conc. (µg/ml)	
NSP1	DA103	1st	0.38	1:200 / 1.9	
NSP2	DA105	1st	0.15	1:200 / 0.75	
NSP3 (743-1072)	DA126	1st	0.13	1:200 / 0.65	
NSP5	DA118	1st	0.35	1:200 / 1.75	
NSP7	DA093	2nd	0.23	1:200 / 1.15	
NSP8	DA110	1st	0.44	1:200 / 2.2	
NSP9	DA094	2nd	0.33	1:200 / 1.65	
NSP10	DA091	2nd	0.27	1:200 / 1.35	

NSP11/12	DA119	1st	0.2	1:200 / 1	
NSP13	DA111	1st	0.29	1:200 / 1.45	
NSP14	DA112	1st	0.22	1:200 / 1.1	
NSP15	DA120	1st	0.14	1:200 / 0.7	
NSP16	DA113	1st	0.36	1:200 / 1.8	
S (ORF2)	DA123	5th	1.05	1:200 / 5.25	
S (RBD, ORF2)	DA125	5th	0.18	1:200 / 0.9	
ORF3A	DA102	1st	0.2	1:200 / 1	
ORF3B	DA100	2nd	0.24	1:200 / 1.2	
E (ORF4)	DA108	1st	0.12	1:200 / 0.6	
M (ORF5)	DA107	1st	0.15	1:200 / 0.75	
ORF6	DA087	2nd	0.14	1:200 / 0.7	
ORF7A	DA124	1st	0.32	1:200 / 1.6	
ORF7B	DA092	2nd	0.17	1:200 / 0.85	
ORF8	DA088	2nd	0.12	1:200 / 0.6	
N (ORF9)	DA114	1st	0.32	1:200 / 1.6	
N (ORF9)	DA114	4th	0.32		1:200 / 1.6
ORF9B	DA089	2nd	0.28	1:200 / 1.4	
ORF9C	DA101	2nd	0.35	1:200 / 1.75	
ORF10	DA090	2nd	0.21	1:200 / 1.05	

Confocal Imaging

Caki-1 cells were seeded in clear-bottom Lumox plates (Sarstedt) one day prior to infection with EDB-2 at MOI = 1. At 16 hpi the cells were fixed with 4% formaldehyde and permeabilized using 0.1% Triton-X-100. Using standard immunocytochemistry techniques, primary antibodies targeting SARS-CoV-2 proteins were used at indicated dilutions / concentrations (Table 1, MRC PPU Dundee) before staining with Donkey anti-Sheep AF488 Secondary Antibody (Invitrogen) at 1:2000, DAPI (Invitrogen, A-11015) at 0.2 µg/ml, and Alexa Fluor™ 594 Phalloidin (Invitrogen) at 1:5,000. The cells were analyzed on a Zeiss LSM 880 Airyscan microscope acquiring z-stack images with a set 0.5 µm imaging interval in the z-direction. Imaging properties were set for an uninfected, stained control sample for each antibody. Images were processed using Fiji (ImageJ) to generate maximum projection images, merge, and montage.

Receptor Quantification

RNA was extracted from Caki-1 cells using the RNeasy (Qiagen) kit according to the manufacturer's instructions. RNA was quantified by Nanodrop and Qubit (ThermoFisher). RT-qPCR reactions using the GoTaq 1-Step RT-qPCR kit (Promega) were set-up to 10 µl final reaction volumes according to the manufacturer's instructions containing 250 nM of each receptors primer pairs and 10 ng of RNA. The RT-qPCR was run on a Mx3000P (Agilent) using an annealing temperature of 60°C and analyzed against a standard curve of Mitochondrial 18S ribosomal RNA (RRN18S) before being normalized to the RRN18 value. Primers used were ACE2

679 (fwd: TTCCACTCTCATTTGAGCCTG, rev: GCCGGAGATAGGAGTGGA), TMPRSS2 (fwd:
680 AGGGAAGACCTCAGAAGTGC, rev: CACAGATCATGGCTGGTGTG), NRP1 (fwd:
681 TCCTCATCGGGCATTCTCTC, rev: TCTGAGACACTGCTCTGCAA, ANPEP (fwd:
682 TTCAACATCACGCTTATCCACC, rev: AGTCGAACTCACTGACAATGAAG), DPP4 (fwd:
683 TACAAAAGTGACATGCCTCAGTT, rev: TGTGTAGAGTATAGAGGGGCAGA), and RRN18S (fwd:
684 AGAAACGGCTACCACATCCA, rev: CACCAGACTTGCCCTCCA).

685 **Receptor siRNA knockdown**

686 siRNA (Dharmacon – Table 2) and Dharmafect 1 (Horizon) were combined in OptiMEM (Gibco)
687 to achieve a final concentration of 20 nM and 0.1% respectively. Transfection complexes were
688 incubated for 20 minutes at room temperature before the addition of 20,000 cells per 96-well. At
689 72 h post transfection, cells were infected with EDB-2 at MOI = 0.1. At 24 and 48 hpi, supernatant
690 was harvested, lysed, and quantified as as previously described [53]. Relative quantities were
691 normalized to the Non-targeting control (#1).

692 *Table 2: Dharmacon siRNA sequences used in this study.*

Gene	siRNA sequence (sense)
ACE2	GAACAUACCUUUGAAGAGA, GCACAAAGGUGACAAUGGA, GGAGGUGGAUGGUCUUUAA, GAGAGGAGACUAUGAAGUA
TMPRSS2	GCAAUGUCGAUAUCUAUAA, GCUAUUGGACCUUACUAUG, ACGGGAAUGUGAUGGUAUU, CGGACUGGAUUUAUCGACA
NRP1	GACCAGGACUACAGGGUUA, GAGGACGGCAUGAGACUUA, CCAGGUGUAUUCCGAACUU, GCCGAGGACCCGAAGGUUA
Cathepsin B	GGAUCACUGUGGAAUCGAA, GGAACUUCUGGACAAGAAA, GGAUGAGCUGGUCAACUAU, GGCACAACUUCUACAACGU
Cathepsin L	CAGCUACUCUAACAUUUGA, UCCAGUAUGUUCAGGAUAA, GGAGAAACCAUUGUGGAAU, CAGAUUAUACGGCAUGAAU
Non-Targeting (control #1)	UAGCGACUAAACACAUCAA, UAAGGCUAUGAAGAGAUAC, AUGUAUUGGCCUGUAUUAG, AUGAACGUGAAUUGCUCAA
SARs2 N protein	AGAACAAACCCAAGGAAAUUU

693

694 **Cell Viability Assay**

695 Caki-1 cells were seeded onto a black-sided, clear-bottomed 96-well plates after reverse
696 transfection with siRNA (20 nM, as described above) and incubated for 72 h. CellTiter-Blue
697 (Promega, G8080) reagent was added to each well at a 1:10 ratio. Following 3 hours of incubation
698 at 37°C, fluorescence as a result of metabolic activity was measured using the BMG Clariostar
699 plate reader (excitation: 545-20, emission: 600-40, 30 flashes/well, bottom optic) and
700 fluorescence intensity was compared between the untreated and the drug treated cells to
701 calculate a percentage viability.

702 **HEK-Blue Interferon Assay**

703 Caki-1 cells were seeded in a 12-well plate and stimulated by either reverse transfecting with
704 Poly I:C (Enzo) using Dharmafect 1 (working concentration of 0.1%), or with media containing
705 Poly I:C (Enzo) or LPS (Sigma) at the indicated concentrations. At 24 hours post treatment,
706 supernatant was harvested and 20 µl added to confluent HEK-Blue IFNα/β cells for 24 h. 20 µl of
707 induced HEK-Blue cell supernatant was added to a corresponding plate with 180 µL of
708 Quanti-Blue substrate in each well. After 3 h incubation SEAP levels were detected using the
709 Clariostar (BMG) at 640 nm.

710 **Figure Legends**

711 **Figure 1: Time course assays in coronaviruses comparing the most commonly used cell**
712 **line with Caki-1.** For all graphs: circle points = MOI 10, square points = MOI 1, triangle points =
713 MOI 0.1, diamond points = MOI 0.01, and the darker the color the higher the MOI, error bars
714 indicate +/- SEM. [A] Time course infection of SARS-CoV-2 variants on Vero E6 and Caki-1 cells,
715 biological n=3x3. Measured through RT-qPCR for the SARS-CoV-2 N gene in the supernatant,
716 samples taken at 0, 6, 16, 24, 48, 72, 96 and 120 hpi at MOIs of 10, 1 and 0.1. [B] Time course
717 infection of MERS-CoV on Huh-7 and Caki-1 cells, biological n=3x3, measured through TCID50 on
718 Huh-7 cells. Samples taken at 24h intervals until 96hpi. [C] GFP time course of infection for
719 hCoV-229E on Huh-7 and Caki-1 cells, measured from 0 hpi to 78 hpi in 6 h intervals, with
720 fluorescence as a proxy for viral replication, biological n=3x3. [D] Fluorescence-activated cell
721 sorting to determine the percentage of infected SARS-CoV-2 cells in Vero E6, Caki-1, Calu-3 and
722 Calu-3-ACE2 cells. Vero E6 and Caki-1 cells were fixed at 17 hpi, stained for intracellular SARS-
723 CoV-2 N protein and sorted for fluorescent cells, biological n=3x3. The same was conducted for
724 Calu-3 and Calu-3-ACE2 cells at 24 hpi and 48 hpi, biological n=3x3.

725 **Figure 2: Confocal analysis of Caki-1 cells showing localization and size of SARS-CoV-2 orf**
726 **proteins.** [A] SARS-CoV-2 genome illustrating the proteins translated by the viral genome and
727 their relative sizes. [B] Immunocytochemsitry staining showing infected and uninfected Caki-1
728 cells stained for SARS-CoV-2 open reading frame proteins. The protein of interest (POI) is
729 indicated in green, the DAPI indicating DNA and RNA in blue, and actin in red. Scale bar represents
730 20 μM.

731 **Figure 3: Confocal analysis of Caki-1 cells showing localisation and size of SARS-CoV-2 NSP**
732 **proteins.** Immunocytochemsitry staining showing infected and uninfected Caki-1 cells stained
733 for SARS-CoV-2 non-structural proteins. The POI is indicated in green, the DAPI indicating DNA
734 and RNA in blue, and actin in red. Scale bar represents 20 μM.

735 **Figure 4: Characterizing Caki-1 cells in the context of respiratory virus infection with**
736 **receptor and interferon competence profiling.** [A] Violin plots showing mRNA expression of
737 entry factors for the human coronaviruses ACE2, TMPRSS2, NRP1, ANPEP, and DPP4 in Caki-1
738 cells, relative to expression of the housekeeping gene RRN18S. Biological n=3x2. [B] (left) Relative
739 replication of SARS-CoV-2 after knockdown of the entry factors in Caki-1 cells relative to the
740 scrambled siRNA non-targeting at 24 hpi, all knockdowns are significant to a p-value < 0.0001
741 using a one-way ANOVA, biological n=12x3, error bars representing +/-SEM. (right) Cell viability
742 after knockdown of SARS-CoV-2 entry factors for 72 h, dotted line indicates the cut-off for 80%
743 relative cell viability, biological nx3, error bars represent +/-SEM. [C] Box and whiskers plot

744 indicating the interferon α/β stimulation of Caki-1 cells after treatment with LPS and Poly I:C, TF
745 indicates transfection into the cell. Transfection of Poly I:C at 1 μg/ml and 10 μg/ml were
746 significant to 0.0001 and 0.001, respectively, using a one-way ANOVA. [D] Time course of IAV
747 infection in Caki-1 cells (dark red filled squares) compared to MDCK (light red hollow squares)
748 cells. Cells were infected at MOI 0.001 with either H1N1 PR8 or Norway 2018 strains as indicated,
749 time points taken at 0, 12, 24 and 48 hpi and titered on MDCK cells, biological n=3, error bars
750 representing +/-SEM. Significance was calculated using multiple Welch's t-tests: *<0.05, **<0.01,
751 ***<0.001, ****<0.0001. [E] RSV-A2-GFP replication in HEp-2 cells (turquoise hollow squares)
752 compared to Caki-1 cells (dark blue filled squares) every 6 hpi up to 78 hpi monitored by
753 fluorescence of GFP. Biological n=3x3, error bars represent +/-SEM.

754

References

1. de Groot RJB, S. C.; Baric, R.; Enjuanes, L.; Gorbalenya, A. E.; Holmes, K. V.; Perlman, S.; Poon, L.; Rottier, P. J. M.; Talbot, P. J.; Woo, P. C. Y.; Ziebuhr, J. Virus Taxonomy: Ninth Report of the International Committee on Taxonomy of Viruses. In: King AMQA, M. J.; Castens, E. B.; Lefkowitz, E. J., editor. London: Elsevier Academic Press; 2011. p. 806-28.
2. Peiris JS, Lai ST, Poon LL, Guan Y, Yam LY, Lim W, et al. Coronavirus as a possible cause of severe acute respiratory syndrome. Lancet. 2003;361(9366):1319-25. doi: 10.1016/s0140-6736(03)13077-2. PubMed PMID: 12711465; PubMed Central PMCID: PMCPMC7112372.
3. Zaki AM, van Boheemen S, Bestebroer TM, Osterhaus AD, Fouchier RA. Isolation of a novel coronavirus from a man with pneumonia in Saudi Arabia. N Engl J Med. 2012;367(19):1814-20. Epub 20121017. doi: 10.1056/NEJMoa1211721. PubMed PMID: 23075143.
4. Wu P, Hao X, Lau EHY, Wong JY, Leung KSM, Wu JT, et al. Real-time tentative assessment of the epidemiological characteristics of novel coronavirus infections in Wuhan, China, as at 22 January 2020. Euro Surveill. 2020;25(3). doi: 10.2807/1560-7917.ES.2020.25.3.2000044. PubMed PMID: 31992388; PubMed Central PMCID: PMCPMC6988272.
5. Pommerenke C, Rand U, Uphoff CC, Nagel S, Zaborski M, Hauer V, et al. Identification of cell lines CL-14, CL-40 and CAL-51 as suitable models for SARS-CoV-2 infection studies. PLoS One. 2021;16(8):e0255622. Epub 2021/08/03. doi: 10.1371/journal.pone.0255622. PubMed PMID: 34339474; PubMed Central PMCID: PMCPMC8328321 a non-profit institute, which distributes the cell lines used in this study. The remaining authors declare that the research was conducted in the absence of any commercial or financial relationships that could be construed as a potential conflict of interest. This does not alter our adherence to PLOS ONE policies on sharing data and materials.
6. Desmyter J, Melnick JL, Rawls WE. Defectiveness of interferon production and of rubella virus interference in a line of African green monkey kidney cells (Vero). Journal of virology. 1968;2(10):955-61. doi: 10.1128/JVI.2.10.955-961.1968. PubMed PMID: 4302013; PubMed Central PMCID: PMCPMC375423.
7. Ogando NS, Dalebout TJ, Zevenhoven-Dobbe JC, Limpens RWAL, van der Meer Y, Caly L, et al. SARS-coronavirus-2 replication in Vero E6 cells: replication kinetics, rapid adaptation and cytopathology. The Journal of general virology. 2020;101(9):925-40. doi: 10.1099/jgv.0.001453. PubMed PMID: 32568027; PubMed Central PMCID: PMCPMC7654748.
8. Chu H, Chan JF, Yuen TT, Shuai H, Yuan S, Wang Y, et al. Comparative tropism, replication kinetics, and cell damage profiling of SARS-CoV-2 and SARS-CoV with implications for clinical manifestations, transmissibility, and laboratory studies of COVID-19: an observational study. Lancet Microbe. 2020;1(1):e14-e23. Epub 20200421. doi: 10.1016/S2666-5247(20)30004-5. PubMed PMID: 32835326; PubMed Central PMCID: PMCPMC7173822.
9. Wei J, Alfajaro MM, DeWeirdt PC, Hanna RE, Lu-Culligan WJ, Cai WL, et al. Genome-wide CRISPR Screens Reveal Host Factors Critical for SARS-CoV-2 Infection. Cell. 2021;184(1):76-91 e13. Epub 20201020. doi: 10.1016/j.cell.2020.10.028. PubMed PMID: 33147444; PubMed Central PMCID: PMCPMC7574718.
10. Zhu Y, Feng F, Hu G, Wang Y, Yu Y, Zhu Y, et al. A genome-wide CRISPR screen identifies host factors that regulate SARS-CoV-2 entry. Nat Commun. 2021;12(1):961. Epub 20210211. doi: 10.1038/s41467-021-21213-4. PubMed PMID: 33574281; PubMed Central PMCID: PMCPMC7878750.
11. Daniloski Z, Jordan TX, Wessels HH, Hoagland DA, Kasela S, Legut M, et al. Identification of Required Host Factors for SARS-CoV-2 Infection in Human Cells. Cell. 2021;184(1):92-105 e16. Epub 20201024. doi: 10.1016/j.cell.2020.10.030. PubMed PMID: 33147445; PubMed Central PMCID: PMCPMC7584921.

12. Schneider WM, Luna JM, Hoffmann HH, Sanchez-Rivera FJ, Leal AA, Ashbrook AW, et al. Genome-Scale Identification of SARS-CoV-2 and Pan-coronavirus Host Factor Networks. Cell. 2021;184(1):120-32 e14. Epub 20201209. doi: 10.1016/j.cell.2020.12.006. PubMed PMID: 33382968; PubMed Central PMCID: PMCPMC7796900.
13. Wang L, Fan X, Bonenfant G, Cui D, Hossain J, Jiang N, et al. Susceptibility to SARS-CoV-2 of Cell Lines and Substrates Commonly Used to Diagnose and Isolate Influenza and Other Viruses. Emerg Infect Dis. 2021;27(5):1380-92. doi: 10.3201/eid2705.210023. PubMed PMID: 33900165; PubMed Central PMCID: PMCPMC8084484.
14. Wang G, Barrett JW, Stanford M, Werden SJ, Johnston JB, Gao X, et al. Infection of human cancer cells with myxoma virus requires Akt activation via interaction with a viral ankyrin-repeat host range factor. Proc Natl Acad Sci U S A. 2006;103(12):4640-5. Epub 20060314. doi: 10.1073/pnas.0509341103. PubMed PMID: 16537421; PubMed Central PMCID: PMCPMC1450224.
15. Lee HL, Essani K. Differential susceptibility of human cancer cell lines to wild-type tanapoxvirus infection. Open Virol J. 2010;4:1-6. Epub 20100408. doi: 10.2174/1874357901004010001. PubMed PMID: 20461227; PubMed Central PMCID: PMCPMC2866450.
16. Rihn SJ, Merits A, Bakshi S, Turnbull ML, Wickenhagen A, Alexander AJT, et al. A plasmid DNA-launched SARS-CoV-2 reverse genetics system and coronavirus toolkit for COVID-19 research. PLoS Biol. 2021;19(2):e3001091. Epub 2021/02/26. doi: 10.1371/journal.pbio.3001091. PubMed PMID: 33630831; PubMed Central PMCID: PMCPMC7906417.
17. McBride CE, Li J, Machamer CE. The cytoplasmic tail of the severe acute respiratory syndrome coronavirus spike protein contains a novel endoplasmic reticulum retrieval signal that binds COPI and promotes interaction with membrane protein. Journal of virology. 2007;81(5):2418-28. Epub 2006/12/15. doi: 10.1128/JVI.02146-06. PubMed PMID: 17166901; PubMed Central PMCID: PMCPMC1865919.
18. Ujike M, Huang C, Shirato K, Makino S, Taguchi F. The contribution of the cytoplasmic retrieval signal of severe acute respiratory syndrome coronavirus to intracellular accumulation of S proteins and incorporation of S protein into virus-like particles. The Journal of general virology. 2016;97(8):1853-64. Epub 20160504. doi: 10.1099/jgv.0.000494. PubMed PMID: 27145752; PubMed Central PMCID: PMCPMC5764123.
19. Lu W, Zheng BJ, Xu K, Schwarz W, Du L, Wong CK, et al. Severe acute respiratory syndrome-associated coronavirus 3a protein forms an ion channel and modulates virus release. Proc Natl Acad Sci U S A. 2006;103(33):12540-5. Epub 20060807. doi: 10.1073/pnas.0605402103. PubMed PMID: 16894145; PubMed Central PMCID: PMCPMC1567914.
20. Zhang Y, Sun H, Pei R, Mao B, Zhao Z, Li H, et al. The SARS-CoV-2 protein ORF3a inhibits fusion of autophagosomes with lysosomes. Cell Discov. 2021;7(1):31. Epub 20210504. doi: 10.1038/s41421-021-00268-z. PubMed PMID: 33947832; PubMed Central PMCID: PMCPMC8096138.
21. Freundt EC, Yu L, Park E, Lenardo MJ, Xu XN. Molecular determinants for subcellular localization of the severe acute respiratory syndrome coronavirus open reading frame 3b protein. Journal of virology. 2009;83(13):6631-40. Epub 20090429. doi: 10.1128/JVI.00367-09. PubMed PMID: 19403678; PubMed Central PMCID: PMCPMC2698541.
22. Konno Y, Kimura I, Uriu K, Fukushi M, Irie T, Koyanagi Y, et al. SARS-CoV-2 ORF3b Is a Potent Interferon Antagonist Whose Activity Is Increased by a Naturally Occurring Elongation Variant. Cell Rep. 2020;32(12):108185. Epub 20200904. doi: 10.1016/j.celrep.2020.108185. PubMed PMID: 32941788; PubMed Central PMCID: PMCPMC7473339.
23. Lee JG, Huang W, Lee H, van de Leemput J, Kane MA, Han Z. Characterization of SARS-CoV-2 proteins reveals Orf6 pathogenicity, subcellular localization, host interactions and

861 attenuation by Selinexor. Cell Biosci. 2021;11(1):58. Epub 2021/03/27. doi:
862 10.1186/s13578-021-00568-7. PubMed PMID: 33766124; PubMed Central PMCID:
863 PMCPMC7993076.
864 24. Miyamoto Y, Itoh Y, Suzuki T, Tanaka T, Sakai Y, Koido M, et al. SARS-CoV-2 ORF6 disrupts
865 nucleocytoplasmic trafficking to advance viral replication. Commun Biol. 2022;5(1):483.
866 Epub 2022/05/20. doi: 10.1038/s42003-022-03427-4. PubMed PMID: 35590097; PubMed
867 Central PMCID: PMCPMC9120032.
868 25. Schaecher SR, Mackenzie JM, Pekosz A. The ORF7b protein of severe acute respiratory
869 syndrome coronavirus (SARS-CoV) is expressed in virus-infected cells and incorporated
870 into SARS-CoV particles. Journal of virology. 2007;81(2):718-31. Epub 20061101. doi:
871 10.1128/JVI.01691-06. PubMed PMID: 17079322; PubMed Central PMCID:
872 PMCPMC1797472.
873 26. Matsuoka K, Imahashi N, Ohno M, Ode H, Nakata Y, Kubota M, et al. SARS-CoV-2 accessory
874 protein ORF8 is secreted extracellularly as a glycoprotein homodimer. The Journal of
875 biological chemistry. 2022;298(3):101724. Epub 2022/02/15. doi:
876 10.1016/j.jbc.2022.101724. PubMed PMID: 35157849; PubMed Central PMCID:
877 PMCPMC8832879.
878 27. Boson B, Legros V, Zhou B, Siret E, Mathieu C, Cosset FL, et al. The SARS-CoV-2 envelope
879 and membrane proteins modulate maturation and retention of the spike protein, allowing
880 assembly of virus-like particles. The Journal of biological chemistry. 2021;296:100111.
881 Epub 20201203. doi: 10.1074/jbc.RA120.016175. PubMed PMID: 33229438; PubMed
882 Central PMCID: PMCPMC7833635.
883 28. Lee HK, Lee BH, Seok SH, Baek MW, Lee HY, Kim DJ, et al. Production of specific antibodies
884 against SARS-coronavirus nucleocapsid protein without cross reactivity with human
885 coronaviruses 229E and OC43. J Vet Sci. 2010;11(2):165-7. doi: 10.4142/jvs.2010.11.2.165.
886 PubMed PMID: 20458159; PubMed Central PMCID: PMCPMC2873818.
887 29. Gordon DE, Jang GM, Bouhaddou M, Xu J, Obernier K, White KM, et al. A SARS-CoV-2 protein
888 interaction map reveals targets for drug repurposing. Nature. 2020;583(7816):459-68.
889 Epub 20200430. doi: 10.1038/s41586-020-2286-9. PubMed PMID: 32353859; PubMed
890 Central PMCID: PMCPMC7431030.
891 30. Shi CS, Qi HY, Boularan C, Huang NN, Abu-Asab M, Shelhamer JH, et al. SARS-coronavirus
892 open reading frame-9b suppresses innate immunity by targeting mitochondria and the
893 MAVS/TRAF3/TRAF6 signalosome. J Immunol. 2014;193(6):3080-9. Epub 20140818. doi:
894 10.4049/jimmunol.1303196. PubMed PMID: 25135833; PubMed Central PMCID:
895 PMCPMC4179872.
896 31. Redondo N, Zaldívar-López S, Garrido JJ, Montoya M. SARS-CoV-2 Accessory Proteins in
897 Viral Pathogenesis: Knowns and Unknowns. Front Immunol. 2021;12:708264. Epub
898 20210707. doi: 10.3389/fimmu.2021.708264. PubMed PMID: 34305949; PubMed Central
899 PMCID: PMCPMC8293742.
900 32. Cornillez-Ty CT, Liao L, Yates JR, Kuhn P, Buchmeier MJ. Severe acute respiratory syndrome
901 coronavirus nonstructural protein 2 interacts with a host protein complex involved in
902 mitochondrial biogenesis and intracellular signaling. Journal of virology.
903 2009;83(19):10314-8. Epub 20090729. doi: 10.1128/JVI.00842-09. PubMed PMID:
904 19640993; PubMed Central PMCID: PMCPMC2748024.
905 33. Lei J, Kusov Y, Hilgenfeld R. Nsp3 of coronaviruses: Structures and functions of a large
906 multi-domain protein. Antiviral Res. 2018;149:58-74. Epub 20171108. doi:
907 10.1016/j.antiviral.2017.11.001. PubMed PMID: 29128390; PubMed Central PMCID:
908 PMCPMC7113668.
909 34. Wang Q, Wu J, Wang H, Gao Y, Liu Q, Mu A, et al. Structural Basis for RNA Replication by the
910 SARS-CoV-2 Polymerase. Cell. 2020;182(2):417-28.e13. Epub 20200522. doi:
911 10.1016/j.cell.2020.05.034. PubMed PMID: 32526208; PubMed Central PMCID:
912 PMCPMC7242921.
913 35. Lin S, Chen H, Chen Z, Yang F, Ye F, Zheng Y, et al. Crystal structure of SARS-CoV-2 nsp10
914 bound to nsp14-ExoN domain reveals an exoribonuclease with both structural and

915 functional integrity. Nucleic Acids Res. 2021;49(9):5382-92. doi: 10.1093/nar/gkab320.
916 PubMed PMID: 33956156; PubMed Central PMCID: PMCPMC8136770.
917 36. Yadav R, Chaudhary JK, Jain N, Chaudhary PK, Khanra S, Dhamija P, et al. Role of Structural
918 and Non-Structural Proteins and Therapeutic Targets of SARS-CoV-2 for COVID-19. Cells.
919 2021;10(4). Epub 20210406. doi: 10.3390/cells10040821. PubMed PMID: 33917481;
920 PubMed Central PMCID: PMCPMC8067447.
921 37. Zillessen P, Celner J, Kretschmann A, Pfeifer A, Racke K, Mayer P. Metabolic role of
922 dipeptidyl peptidase 4 (DPP4) in primary human (pre)adipocytes. Sci Rep. 2016;6:23074.
923 Epub 2016/03/18. doi: 10.1038/srep23074. PubMed PMID: 26983599; PubMed Central
924 PMCID: PMCPMC4794806.
925 38. Hasan MR, Ahmad MN, Dargham SR, Zayed H, Al Hashemi A, Ngwabi N, et al.
926 Nasopharyngeal Expression of Angiotensin-Converting Enzyme 2 and Transmembrane
927 Serine Protease 2 in Children within SARS-CoV-2-Infected Family Clusters. Microbiol
928 Spectr. 2021;9(3):e0078321. Epub 20211103. doi: 10.1128/Spectrum.00783-21. PubMed
929 PMID: 34730438; PubMed Central PMCID: PMCPMC8567246.
930 39. Gao J, Aksoy BA, Dogrusoz U, Dresdner G, Gross B, Sumer SO, et al. Integrative analysis of
931 complex cancer genomics and clinical profiles using the cBioPortal. Sci Signal.
932 2013;6(269):pl1. Epub 2013/04/04. doi: 10.1126/scisignal.2004088. PubMed PMID:
933 23550210; PubMed Central PMCID: PMCPMC4160307.
934 40. Cerami E, Gao J, Dogrusoz U, Gross BE, Sumer SO, Aksoy BA, et al. The cBio cancer genomics
935 portal: an open platform for exploring multidimensional cancer genomics data. Cancer
936 Discov. 2012;2(5):401-4. Epub 2012/05/17. doi: 10.1158/2159-8290.CD-12-0095.
937 PubMed PMID: 22588877; PubMed Central PMCID: PMCPMC3956037.
938 41. Mautner L, Hoyos M, Dangel A, Berger C, Ehrhardt A, Baiker A. Replication kinetics and
939 infectivity of SARS-CoV-2 variants of concern in common cell culture models. Virol J.
940 2022;19(1):76. Epub 2022/04/28. doi: 10.1186/s12985-022-01802-5. PubMed PMID:
941 35473640; PubMed Central PMCID: PMCPMC9038516.
942 42. Schulze H, Bayer W. Changes in Symptoms Experienced by SARS-CoV-2-Infected Individuals
943 – From the First Wave to the Omicron Variant. Frontiers in Virology. 2022;2. doi:
944 10.3389/fviro.2022.880707.
945 43. Meng B, Abdullahi A, Ferreira I, Goonawardane N, Saito A, Kimura I, et al. Altered TMPRSS2
946 usage by SARS-CoV-2 Omicron impacts infectivity and fusogenicity. Nature.
947 2022;603(7902):706-14. Epub 2022/02/02. doi: 10.1038/s41586-022-04474-x. PubMed
948 PMID: 35104837; PubMed Central PMCID: PMCPMC8942856.
949 44. Tseng CT, Tseng J, Perrone L, Worthy M, Popov V, Peters CJ. Apical entry and release of
950 severe acute respiratory syndrome-associated coronavirus in polarized Calu-3 lung
951 epithelial cells. Journal of virology. 2005;79(15):9470-9. Epub 2005/07/15. doi:
952 10.1128/JVI.79.15.9470-9479.2005. PubMed PMID: 16014910; PubMed Central PMCID:
953 PMCPMC1181546.
954 45. You J, Dove BK, Enjuanes L, DeDiego ML, Alvarez E, Howell G, et al. Subcellular localization
955 of the severe acute respiratory syndrome coronavirus nucleocapsid protein. The Journal of
956 general virology. 2005;86(Pt 12):3303-10. doi: 10.1099/vir.0.81076-0. PubMed PMID:
957 16298975.
958 46. Yuan X, Li J, Shan Y, Yang Z, Zhao Z, Chen B, et al. Subcellular localization and membrane
959 association of SARS-CoV 3a protein. Virus Res. 2005;109(2):191-202. doi:
960 10.1016/j.virusres.2005.01.001. PubMed PMID: 15763150; PubMed Central PMCID:
961 PMCPMC7114198.
962 47. Miserey-Lenkei S, Trajkovic K, D'Ambrosio JM, Patel AJ, Čopič A, Mathur P, et al. A
963 comprehensive library of fluorescent constructs of SARS-CoV-2 proteins and their initial
964 characterisation in different cell types. Biol Cell. 2021;113(7):311-28. Epub 20210510. doi:
965 10.1111/boc.202000158. PubMed PMID: 33666950; PubMed Central PMCID:
966 PMCPMC8014678.
967 48. Cervantes-Barragan L, Zust R, Maier R, Sierro S, Janda J, Levy F, et al. Dendritic cell-specific
968 antigen delivery by coronavirus vaccine vectors induces long-lasting protective antiviral

969 and antitumor immunity. mBio. 2010;1(4). Epub 2010/09/17. doi: 10.1128/mBio.00171-
970 10. PubMed PMID: 20844609; PubMed Central PMCID: PMCPMC2939679.
971 49. Hallak LK, Collins PL, Knudson W, Peeples ME. Iduronic acid-containing
972 glycosaminoglycans on target cells are required for efficient respiratory syncytial virus
973 infection. Virology. 2000;271(2):264-75. Epub 2000/06/22. doi: 10.1006/viro.2000.0293.
974 PubMed PMID: 10860881.
975 50. Kindler E, Jonsdottir HR, Muth D, Hamming OJ, Hartmann R, Rodriguez R, et al. Efficient
976 replication of the novel human betacoronavirus EMC on primary human epithelium
977 highlights its zoonotic potential. mBio. 2013;4(1):e00611-12. Epub 2013/02/21. doi:
978 10.1128/mBio.00611-12. PubMed PMID: 23422412; PubMed Central PMCID:
979 PMCPMC3573664.
980 51. Kratzel A, Kelly JN, V'Kovski P, Portmann J, Bruggemann Y, Todt D, et al. A genome-wide
981 CRISPR screen identifies interactors of the autophagy pathway as conserved coronavirus
982 targets. PLoS Biol. 2021;19(12):e3001490. Epub 2021/12/29. doi:
983 10.1371/journal.pbio.3001490. PubMed PMID: 34962926; PubMed Central PMCID:
984 PMCPMC8741300.
985 52. de Wit E, Spronken MI, Bestebroer TM, Rimmelzwaan GF, Osterhaus AD, Fouchier RA.
986 Efficient generation and growth of influenza virus A/PR/8/34 from eight cDNA fragments.
987 Virus Res. 2004;103(1-2):155-61. Epub 2004/05/28. doi: 10.1016/j.virusres.2004.02.028.
988 PubMed PMID: 15163504.
989 53. Craig N, Fletcher SL, Daniels A, Newman C, O'Shea M, Tan WS, et al. Direct Lysis RT-qPCR of
990 SARS-CoV-2 in Cell Culture Supernatant Allows for Fast and Accurate Quantification.
991 Viruses. 2022;14(3). Epub 2022/03/27. doi: 10.3390/v14030508. PubMed PMID:
992 35336915; PubMed Central PMCID: PMCPMC8949636.
993

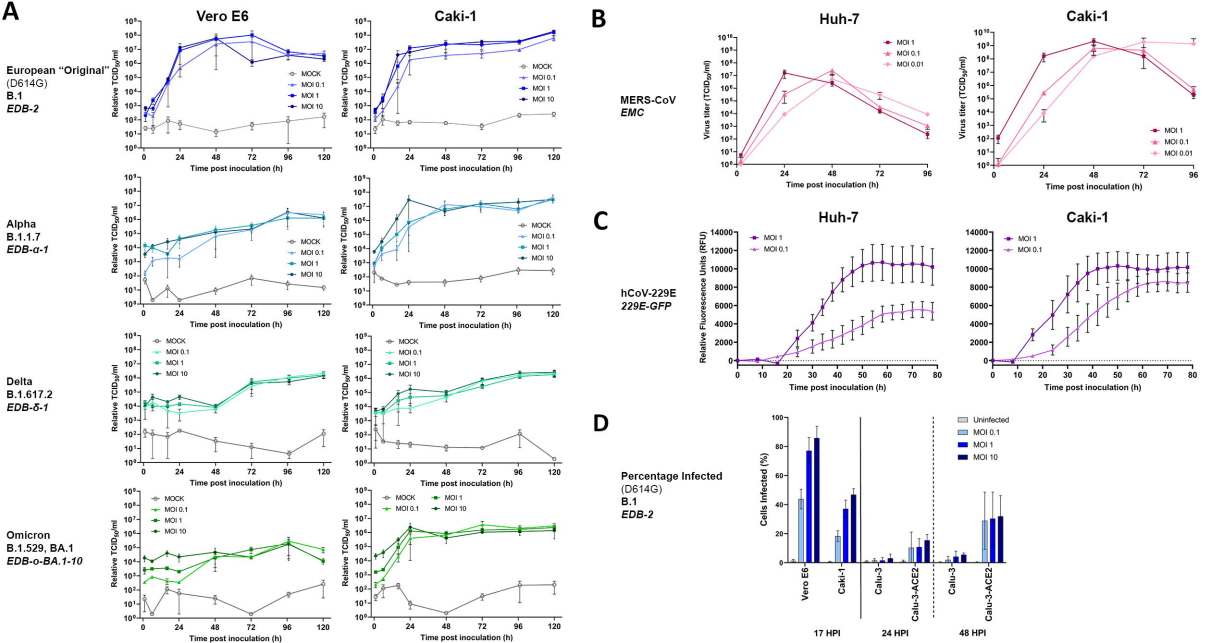
A
Vero E6
Caki-1
European "Original"
(D614G)
B.1
EDB-2
Alpha
B.1.1.7
EDB-α-1
Delta
B.1.617.2
EDB-δ-1
Omicron
B.1.529, BA.1
EDB-o-BA.1-10
MOCK
MOI 0.1
MOI 1
MOI 10
Relative TCID50/ml
Time post inoculation (h)
B
Huh-7
Caki-1
MERS-CoV
EMC
MOI 1
MOI 0.1
MOI 0.01
Virus titer (TCID50/ml)
Time post inoculation (h)
C
Huh-7
Caki-1
hCoV-229E
229E-GFP
MOI 1
MOI 0.1
Relative Fluorescence Units (RFU)
Time post inoculation (h)
D
Percentage Infected
(D614G)
B.1
EDB-2
Uninfected
MOI 0.1
MOI 1
MOI 10
Cells Infected (%)
Vero E6
Caki-1
Calu-3
Calu-3-ACE2
Calu-3
Calu-3-ACE2
17 HPI
24 HPI
48 HPI

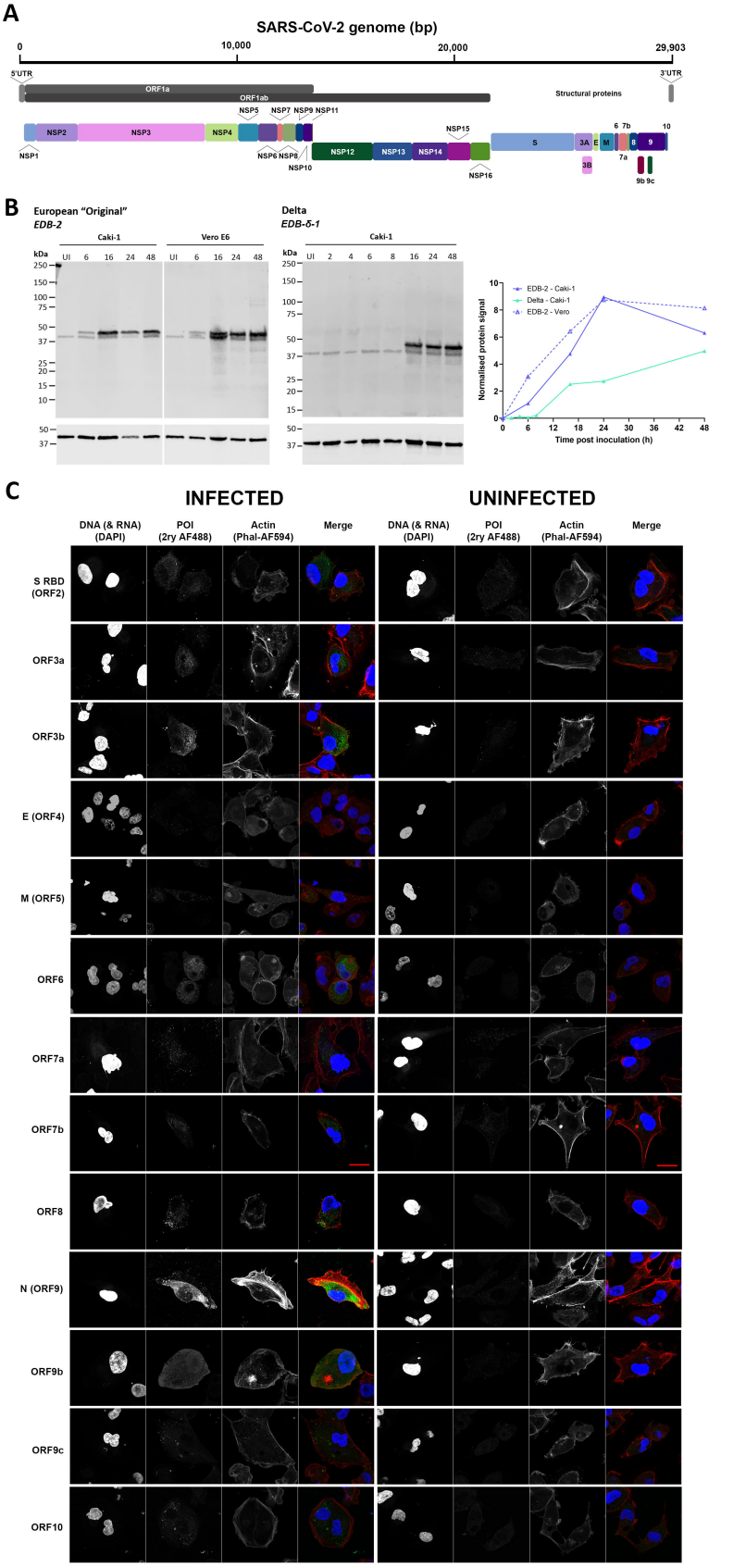
A
SARS-CoV-2 genome (bp)
0
10,000
20,000
29,903
5'UTR
3'UTR
ORF1a
ORF1ab
Structural proteins
NSP1
NSP2
NSP3
NSP4
NSP5
NSP6
NSP7
NSP8
NSP9
NSP10
NSP11
NSP12
NSP13
NSP14
NSP15
NSP16
S
3A
3B
E
M
6
7a
7b
8
9
9b
9c
10
B
European "Original"
EDB-2
Caki-1
Vero E6
kDa
UI
6
16
24
48
Delta
EDB-δ-1
Caki-1
UI
2
4
6
8
16
24
48
EDB-2 - Caki-1
Delta - Caki-1
EDB-2 - Vero
Normalised protein signal
Time post inoculation (h)
C
INFECTED
UNINFECTED
DNA (& RNA) (DAPI)
POI (2ry AF488)
Actin (Phal-AF594)
Merge
S RBD (ORF2)
ORF3a
ORF3b
E (ORF4)
M (ORF5)
ORF6
ORF7a
ORF7b
ORF8
N (ORF9)
ORF9b
ORF9c
ORF10

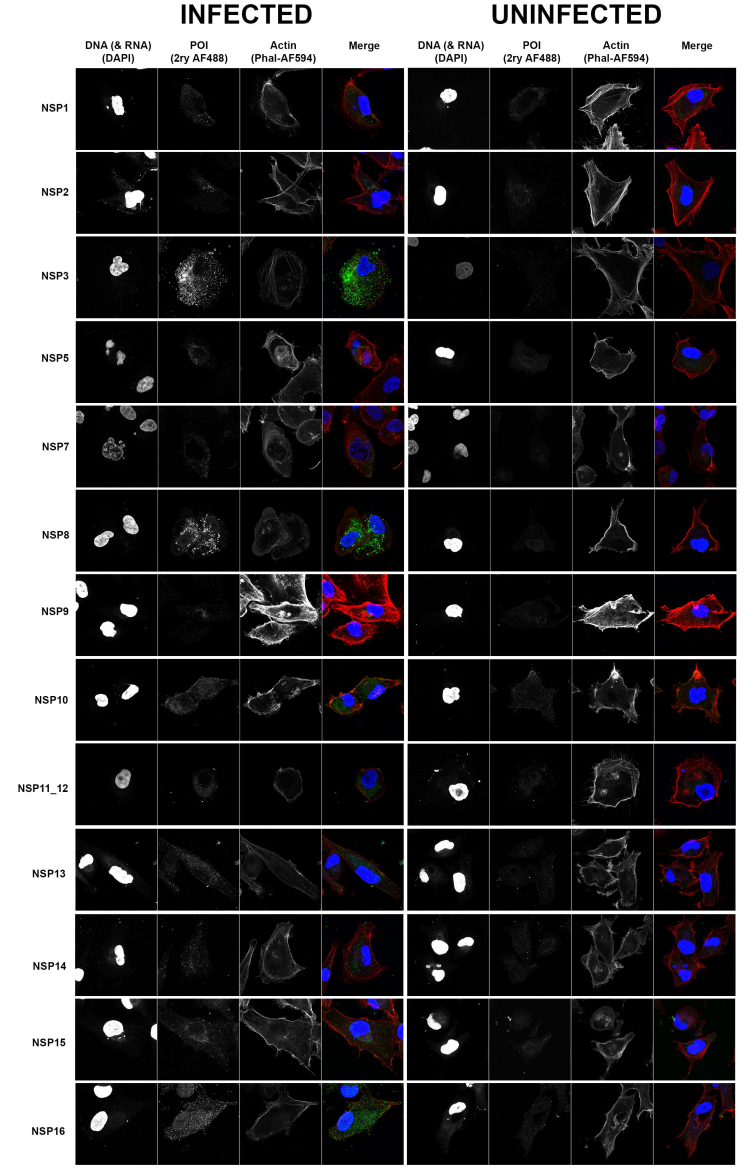
INFECTED
UNINFECTED
DNA (& RNA) (DAPI)
POI (2ry AF488)
Actin (Phal-AF594)
Merge
NSP1
NSP2
NSP3
NSP5
NSP7
NSP8
NSP9
NSP10
NSP11_12
NSP13
NSP14
NSP15
NSP16

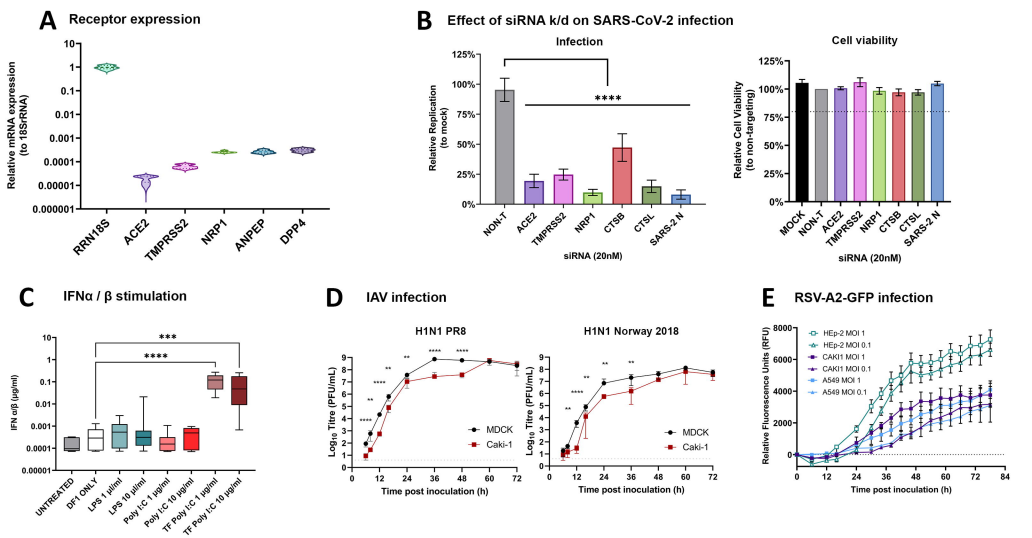
A
Receptor expression
Relative mRNA expression (to 18S-RNA)
10
1
0.1
0.01
0.001
0.0001
0.00001
0.000001
RRN18S
ACE2
TMPRSS2
NRP1
ANPEP
DPP4
B
Effect of siRNA k/d on SARS-CoV-2 infection
Infection
Relative Replication (to mock)
125%
100%
75%
50%
25%
0%
****
NON-T
ACE2
TMPRSS2
NRP1
CTSB
CTSL
SARS-2 N
siRNA (20nM)
Cell viability
Relative Cell Viability (to non-targeting)
125%
100%
75%
50%
25%
0%
MOCK
NON-T
ACE2
TMPRSS2
NRP1
CTSB
CTSL
SARS-2 N
siRNA (20nM)
C
IFNα / β stimulation
IFN α/β (µg/ml)
10
1
0.1
0.01
0.001
0.0001
0.00001
***
****
UNTREATED
DF1 ONLY
LPS 1 µl/ml
LPS 10 µl/ml
Poly I:C 1 µg/ml
Poly I:C 10 µg/ml
TF Poly I:C 1 µg/ml
TF Poly I:C 10 µg/ml
D
IAV infection
H1N1 PR8
Log10 Titre (PFU/mL)
Time post inoculation (h)
MDCK
Caki-1
H1N1 Norway 2018
Log10 Titre (PFU/mL)
Time post inoculation (h)
MDCK
Caki-1
E
RSV-A2-GFP infection
Relative Fluorescence Units (RFU)
8000
6000
4000
2000
0
HEp-2 MOI 1
HEp-2 MOI 0.1
CAKI1 MOI 1
CAKI1 MOI 0.1
A549 MOI 1
A549 MOI 0.1
Time post inoculation (h)